Supplementary Materials for

De novo design of protein logic gates

Zibo Chen*, Ryan D. Kibler†, Andrew Hunt†, Florian Busch†, Jocelynn Pearl†‡, Mengxuan Jia, Zachary L. VanAernum, Basile I. M. Wicky, Galen Dods, Hanna Liao‡, Matthew Wilken, Christie Ciarlo, Shon Green, Hana El-Samad, John Stamatoyannopoulos, Vicki H. Wysocki, Michael C. Jewett, Scott E. Boyken‡, David Baker§

*Present address: Division of Biology and Biological Engineering, California Institute of Technology, Pasadena, CA 91125, USA.
†These authors contributed equally to this work.
‡Present address: Lyell Immunopharma, Inc., Seattle, WA 98109, USA.
§Corresponding author. Email: dabaker@uw.edu

Published 3 April 2020, *Science* **368**, 78 (2020)
DOI: 10.1126/science.aay2790

This PDF file includes:

Other Supplementary Material for this manuscript includes the following:
(available at science.sciencemag.org/content/368/6486/78/suppl/DC1)

Table S1 (.xlsx)
Vector Maps (.zip)

Materials and Methods

Buffer and media recipe for protein expression and yeast-two-hybrid experiments

TBM-5052

1.2% [wt/vol] tryptone, 2.4% [wt/vol] yeast extract, 0.5% [wt/vol] glycerol, 0.05% [wt/vol] D-glucose, 0.2% [wt/vol] D-lactose, 25 mM Na_2HPO_4, 25 mM KH_2PO_4, 50 mM NH_4Cl, 5 mM Na_2SO_4, 2 mM $MgSO_4$, 10 µM $FeCl_3$, 4 µM $CaCl_2$, 2 µM $MnCl_2$, 2 µM $ZnSO_4$, 400 nM $CoCl_2$, 400 nM $NiCl_2$, 400 nM $CuCl_2$, 400 nM Na_2MoO_4, 400 nM Na_2SeO_3, 400 nM H_3BO_3

Lysis buffer

20 mM Tris, 300 mM NaCl, 20 mM Imidazole, pH 8.0 at room temperature

Wash buffer

20 mM Tris, 300mM NaCl, 30 mM Imidazole, pH 8.0 at room temperature

Elution buffer

20 mM Tris, 300 mM NaCl, 250 mM Imidazole, pH 8.0 at room temperature

TBS buffer

20 mM Tris pH 8.0, 100 mM NaCl

YPAD buffer

Peptone 20 g/L, yeast extract10 g/L, Adenine hemisulfate 10 µg/L, dextrose (20 g/L)

C-Trp-Ura-Leu-His+Adenine hemisulfate+Glucose

Yeast nitrogen base w/o amino acids (6.7 g/L), synthetic DO media (-Leu/-His/-Trp/-Ura) (1.4 g/L), dextrose (20 g/L), adenine hemisulfate (10 µg/L)

Construction of synthetic genes

For the expression of proteins in *E.coli*, synthetic genes were ordered from Genscript Inc. (Piscataway, N.J., USA) and delivered in pET21-NESG *E. coli* expression vector, inserted between the NdeI and XhoI sites. For each expression construct, a hexahistidine tag followed by a tobacco etch virus (TEV) protease cleavage site (GSSHHHHHHSSGENLYFQGS) were added in frame at the N-terminus of the protein. A stop codon was introduced at the 3' end of the protein coding sequence to prevent expression of the C-terminal hexahistidine tag in the vector.

Genes for yeast-two-hybrid (Y2H) studies were cloned into plasmids bearing the GAL4 DNA-binding domain (poDBD) and the GAL4 transcription activation domain (poAD) (*53*). Input proteins were cloned into plasmids V510 (uracil auxotrophic selection marker) and MX1 (bleomycin selection marker). Genes were expressed under the control of ADH1 promoters.

Genes for NanoBiT assay were ordered from Genscript Inc. (Piscataway, N.J., USA) and were synthesized and cloned into one or more of the following vectors: pJL1, pJL1-lgBiT, pJL1-smBiT, pJL1-lgBiT-sfGFP, pJL1-smBiT-sfGFP, or pJL1-sfGFP. NanoBiT constructs were designed with a c-terminal fusion of either the smBiT or lgBiT fusion partner (114 and 11s respectively (*40*), for sequences see Table S1) with a 15 amino acid linker (GGSGGGGSGGSSSGG) separating the inserted gene and the fusion partner. Where specified, genes were also fused to the c-terminus of sfGFP separated by a 30 amino acid linker (GGGSGSx5). Genes were expressed using a T7 promoter in cell-free protein synthesis.

The fluorescence-reporting yeast two-hybrid-like assay was constructed using hierarchical golden gate assembly (*54*). Split transcription factor modules ((*14*), ZF43_8 and p43_8(8x)) and DHDs were domesticated as parts using PCR amplification or gBlocks (IDT). The progesterone responsive transcription factor (Z3PM) and cognate promoter (pZ3) were domesticated using PCR ((*55*), e.g. Addgene #87944 and #89195, respectively). All other promoters and terminators were taken from (3). Transcriptional units were assembled into cassette vectors and multi-transcriptional units were assembled into integration vectors for insertion into the yeast genome at the indicated loci (see “Progesterone-responsive yeast strain construction and growth media”).

Protein expression

Plasmids were transformed into chemically competent *E. coli* expression strain Lemo21(DE3) (New England Biolabs) for protein expression. Following transformation and overnight growth, single colonies were picked from agar plates into 5 ml Luria-Bertani (LB) medium containing 100 µg/mL carbenicillin (for pET21-NESG vectors) with shaking at 225 rpm for 18 hours at 37°C. Proteins were expressed using the autoinduction method (*56*): starter cultures were further diluted into 500 ml TBM-5052 containing 100 µg/mL carbenicillin, and incubated with shaking at 225 rpm for 24 hours at 37°C.

Affinity purification

E. coli cells were harvested by centrifugation at 5000 rcf for 15 minutes at 4°C and the pellet resuspended in 18 ml lysis buffer. EDTA-free cocktail protease inhibitor (Roche), lysozyme, and DNAse were added to the resuspended cell pellet, followed by cell lysis via sonication at 70% power for 5 minutes. Lysates were clarified by centrifugation at 4°C and 18,000 rpm for 45 minutes and applied to columns containing Ni-NTA (Qiagen) resin pre-equilibrated with lysis buffer. The column was washed two times with 5 column volumes (CV) of wash buffer, followed by 5 CV of elution buffer buffer for protein elution.

Size-exclusion chromatography (SEC)

Eluted proteins were buffer exchanged into lysis buffer. N-terminal hexahistidine tags were removed with TEV protease cleavage overnight at room temperature, at a ratio of 1 mg TEV for 100 mg of protein. After TEV cleavage, sample was passed over a fresh Ni-NTA column and washed with 1.5 CV of lysis buffer, collecting flow through. The resulting proteins were purified by SEC using a Superdex 75 10/300 increase column (GE Healthcare) in TBS buffer.

Circular dichroism (CD) measurements

Circular dichroism (CD) wavelength scans (260 - 195 nm) and temperature melts (25 - 95 °C) were performed using an AVIV model 420 CD spectrometer, with protein samples diluted to 0.25 mg/ml in PBS pH 7.4 in a 0.1-cm cuvette. Temperature melts were carried out at a heating rate of 4 °C/min and monitored by the change in ellipticity at 222 nm.

GdmCl titrations were performed on a JASCO model J-1500 with automated titration apparatus in PBS pH 7.4 at 25 °C, with protein concentrations between 0.08 mg/ml to 0.025 mg/ml in a 1-cm cuvette with stir bar. Each titration consisted of at least 34 evenly distributed GdmCl concentration points up to 7.4 M with 30 seconds of mixing time for each step. Titrant solution consisted of the same concentration of protein in PBS and GdmCl.

CD data analysis and model fitting

Folding free energies were obtained by fitting equilibrium denaturation data. Fused hairpin constructs had biphasic unfolding transitions, indicating the existence of an intermediate on their respective energy landscapes. Since native MS showed that Linker 0, Linker 2, Linker 6, and Linker 12 were almost exclusively monomeric in buffer (figure S3), it was concluded that these intermediates were partially folded monomeric species. Thus, the chemical denaturation data of these proteins was fitted to a unimolecular 3-state model:

$$N \Leftrightarrow I \Leftrightarrow D$$

where N represents the fully folded state, I a partially folded intermediate, and D the denatured state. The fraction of each species can be written as a function of $K_1 = [I]/[N]$ and $K_2 = [D]/[I]$, the equilibrium constants for the first and second transitions respectively:

$$f_N = (1 + K_1 + K_1 \cdot K_2)^{-1}$$

$$f_I = (1 + K_2 + \frac{1}{K_1})^{-1}$$

$$f_D = (1 + \frac{1}{K_2} + \frac{1}{K_1 \cdot K_2})^{-1}$$

In the context of equilibrium chemical denaturation experiments, the free energy of unfolding is a linear function of denaturant concentration:

$$\Delta G_{[den]} = \Delta G_{buffer} - m \cdot [den]$$

where$\Delta G_{[den]}$represents the free energy of the system at a given concentration of denaturant, $\Delta G_{buffer}$is the corresponding free energy change in the absence of denaturant, and m is a constant of proportionality that relates to the change in solvent-accessible surface area upon unfolding ($\Delta SASA$). Thus, the effect of denaturants on the equilibrium constant relating to each transition can be written as a function of its free energy difference in buffer, and a specific *m*-value:

$$K_1 = exp(\frac{m_1 \cdot [den] - \Delta G_1}{R \cdot T})$$

$$K_2 = exp(\frac{m_2 \cdot [den] - \Delta G_2}{R \cdot T})$$

By combining these expressions with the definitions for f_N, f_I, f_D, the fractional distribution of each species can be expressed as a function of denaturant concentration, and the free energy change corresponding to each transition (in buffer). Finally, for an ensemble spectroscopic technique such as CD, the observed signal (the dependent variable) as a function of denaturant concentration (the independent variable) can be expressed as a linear combination of the spectroscopic signals corresponding to each species, weighed by their fractional contribution to the ensemble:

$$MRE_{222nm} = f_N \cdot MRE_N + f_I \cdot MRE_I + f_D \cdot MRE_D$$

Where MRE_N, MRE_I, MRE_Drepresent the spectroscopic signatures (baselines) for the native, intermediate, and denatured states respectively. This equation was used to fit chemical denaturation data for the different linker proteins, and the fitted parameters are reported in Table S3. For Linker 24 in buffer, native MS revealed a significant proportion of dimer (Table S4). Therefore, this model is not entirely appropriate for describing the unfolding, and the fitted values for this construct should be interpreted with care. Nevertheless, denaturation performed at different concentrations of protein revealed that the position of the second transition was concentration-independent, and thus unimolecular. For this event, the model holds.

The total *m*-values for these linked hairpins were found to be around 3 kcal mol^{-1} M^{-1}. It has been shown that *m*-values correlate with $\Delta SASA$ of unfolding (*57*). For the folded state, $SASA$ was estimated from the structures of DHDs (*32*) using PyMOL to be 8800 $Å^2$. For the unfolded state, $SASA$ was estimated using ProtSA (*58*, *59*), and is about 20,000 $Å^2$. Thus, $\Delta SASA$ for the unimolecular unfolding of a fused hairpin should be around 11,000 $Å^2$, which would have a

predicted *m*-value of 3.3. This number is in close agreement with the fitted parameters reported here, in line with the notion that the folded state for these linker proteins has a four helix bundle topology.

Small Angle X-ray Scattering (SAXS)

Protein samples were purified by SEC in 25 mM Tris pH 8.0, 150 mM NaCl and 2% glycerol; elution fractions preceding the void volume of the column were used as blanks for buffer subtraction. Scattering measurements were performed at the SIBYLS 12.3.1 beamline at the Advanced Light Source. The sample-to-detector distance was 1.5 m, and the X-ray wavelength (λ) was 1.27 Å, corresponding to a scattering vector q ($q = 4\pi \sin\theta/\lambda$, where 2θ is the scattering angle) range of 0.01 to 0.3 $Å^{-1}$. A series of exposures were taken of each well, in equal sub-second time slices: 0.3-s exposures for 10 s resulting in 32 frames per sample. For each sample, data were collected for two different concentrations to test for concentration-dependent effects; 'low' concentration samples ranged at 2.5 mg/ml and 'high' concentration samples at 5 mg/ml. Data were processed using the SAXS FrameSlice online serve and analysed using the ScÅtter software package (*35*, *60*). The FoXS online server (*61*, *62*) was used to compare experimental scattering profiles to design models and calculate quality of fit (χ) values.

Yeast two-hybrid assay for logic gates

Chemically competent cells of yeast strain PJ69-4a (MATa trp1-901 leu2-3,112 ura3-52 his3-200 gal4(deleted) gal80(deleted) LYS2::GAL1-HIS3 GAL2-ADE2 met2::GAL7-lacZ) were transformed with the appropriate pair of plasmids containing DNA binding domains (DBD) or activation domains (AD), using the LiAc/SS carrier DNA/PEG method (*63*). For two input CIPHR logic gates, genes encoding the input proteins (together with selection markers) were genetically integrated into either or both of the Ura3 locus (uracil auxotrophic selection marker) or the YCR043 locus

(bleomycin selection marker). In the case of three input CIPHR logic gates, genes encoding two input proteins were genetically integrated as described, with the additional input cloned downstream of either the AD or DBD plasmid, separated by a p2a and nuclear localization sequence (GSGATNFSLLKQAGDVEENPGPGDKAELIPEPPKKKRKVELGTA). The p2a sequence ensures translational cleavage to make the additional input protein a separate protein. The selection of transformed yeast cells was performed in synthetic dropout (SDO) medium lacking tryptophan and leucine for 48 h with shaking at 1,000 r.p.m. at 30 °C. The resulting culture was diluted 1:100 and grown for 16 h in fresh SDO medium lacking tryptophan and leucine, before being diluted 1:100 in fresh SDO medium lacking tryptophan, leucine and histidine. The culture was incubated with shaking at 1,000 r.p.m. at 30 °C. As it is necessary to bring the DBD and the transcription activation domain into proximity for the growth of yeast cells in medium lacking histidine, successful activation of logic gates was indicated by the growth of yeast cells (*64*, *65*). The optical density of yeast cells was recorded at 24 h, 48 h, and 72 h.

Native MS of individual proteins

Sample purity and integrity were determined by online buffer exchange MS using an UltiMate 3000 HPLC coupled to an Exactive Plus EMR Orbitrap instrument (Thermo Fisher Scientific) that was modified to incorporate a quadrupole mass filter and allow for surface-induced dissociation (*66*). Between 10 and 100 pmol protein was injected and online buffer exchanged to 200 mM ammonium acetate (AmAc) by a self-packed buffer exchange column (P6 polyacrylamide gel, BioRad) at a flow-rate of 100 µL per min. Data were deconvoluted with UniDec (version 3.1.1) (*67*) and are shown in Table S4.

Native MS titration assay and data analysis

Titration assay: Protein concentrations were determined based on UV absorbance at 280 nm with a Nanodrop™ 2000c spectrophotometer (Thermo Fisher Scientific). Mixtures for titration were

prepared as outlined in Supplementary Table 5. Other mixtures are mixed with a final monomer concentration at 10 μM for each component. Proteins were incubated at 75 °C for 30 min in the presence of 5 M guanidinium hydrochloride to ensure complete denaturation. The denatured proteins were subsequently refolded into 200 mM AmAc by dialysis using Pierce™ 96-well Microdialysis Plate, 3.5K MWCO (ThermoFisher Scientific). 50 μL of each sample was loaded into individual microdialysis devices with 1.6 mL 200 mM AmAc in each well. The buffer was changed 8 times over a total dialysis time of 36 hours at room temperature. 12.5, 25, and 50 fold dilutions in 200 mM AmAc were prepared. Dilutions were measured in triplicate by flow-injecting 5 μL into an Exactive Plus EMR Orbitrap instrument (Thermo Fisher Scientific) with 200 mM AmAc as flowing carrier stream. Mass spectra were recorded for 1,000 – 8,000 *m/z* at 17,500 resolution as defined at 200 *m/z*. The injection time was set to 200 ms for 1-in AND and 3-in AND titrations, and 150 ms for 2-in AND titrations. Voltages applied to the transfer optics were optimized to allow ion transmission while minimizing unintentional ion activation. Complex formations were observed and are shown in Table S6. Dilution series of individual proteins were also measured to ensure for a linear correlation between signal intensities and protein concentration (Table S7).

Data analysis: All mass spectra were deconvoluted and processed using Intact Mass software (Protein Metrics, Cupertino, CA). Software default deconvolution parameters were used with the exception of minimum charge state (3) and mass range (5,000-80,000 Da). A list of theoretical masses for complexes up to pentamers was generated and included in the Intact Mass software for species assignments. Mass areas (in the mass “zero-charge” domain) were made by setting the mass area integration width to 12 Da. Mass areas of all species were exported from Intact Mass software using the reports function and then combined in Excel to generate titration curves. For Fig. 1G, each dot represents the total amount of any complexes that contain both ***2*** and ***1’-2’*** (e.g., ***1:1’-2’:2***, ***1’-2’:2***), normalized against its maximum value.

Cell-Free extract preparation

E. coli extracts were prepared following an established protocol in literature (*41*), with minor modifications. Briefly, three 150 mL BL21 Star™ (DE3) starter cultures were inoculated in LB from a glycerol stock and cultured in a 250 mL baffled flask at 37 °C for 16 hours. The starter cultures were used to inoculate 10 L of 2xYTPG media (16 g/L tryptone, 10 g/L yeast extract, 5 g/L sodium chloride, 7 g/L potassium phosphate dibasic, 3 g/L potassium phosphate monobasic, 18 g/L glucose) in a Sartorious BIOSTAT® Cplus fermenter at an initial OD600 of 0.08. The 2xYTP was prepared lacking glucose in 75% of the final volume and sterilized using the fermenter sterilization cycle. A 4x glucose solution was prepared and autoclaved separately, then added to the fermenter. Cells were cultured at 37 °C with an air flow rate of 8 SLPM and a 600 RPM stir rate.

Cultures were grown until OD600 0.4-0.6, at which point the expression of T7 RNA polymerase was induced by the addition of IPTG to a final concentration of 0.5 mM. Cells were harvested at an OD600 of 3.0 via centrifugation at 5,000g for 10 minutes at 4 °C. Cell pellets were washed twice with 25 mL S30 buffer per 50 mL culture (10 mM Tris Acetate pH 8.2, 14 mM Magnesium Acetate, and 60 mM Potassium Acetate), centrifuging at 5,000g and 7,000g for the first and second washes respectively. Pellets were flash frozen in liquid nitrogen for storage. Pellets were thawed on ice for 1 hour and resuspended in 1 mL S30 buffer plus dithiothreitol per gram of cell mass (10 mM tris acetate pH 8.2, 14 mM magnesium acetate, and 60 mM potassium acetate, 2 mM dithiothreitol). Cell suspensions were lysed using an Avestin EmulsiFlex®-C3 Homogenizer at a lysis pressure of 23,000 PSI. Cell debris was separated via centrifugation at 10,000g for 10 minutes, and the clarified lysate was collected, flash frozen in liquid nitrogen, and stored at -80 °C.

Cell-Free Protein Synthesis reactions

CFPS reactions utilized the PANOx-SP system (*68*). CFPS reactions were composed of the following reagents: 12 mM magnesium glutamate, 10 mM ammonium glutamate, 130 mM potassium glutamate, 1.2 mM ATP, 0.5 mM of each CTP, GTP, and UTP. 0.03 mg/mL folinic acid, 0.17 mg/mL *E. coli* MRE600 tRNA (Roche 10109541001), 100 mM NAD, 50 mM CoA, 4 mM oxalic acid, 1 mM putrescine, 1 mM spermidine, 57 mM HEPES pH 7.2, 2 mM of each amino acid, 33.3 mM PEP, 30% v/v *E. coli* extract, linear DNA templates were added to a final concentration of 3.33 µM, and the remainder water. For reactions co-expressing multiple proteins, each template was added to a final concentration of 0.83 µM. The preparation of these reagents has been described in detail elsewhere (*69*). All reaction components were assembled on ice and 12 µL reactions were pipetted into 1.5 mL microtubes. Reactions were allowed to proceed at 30 °C for 20 hours. Protein expression yields were quantified by the addition of 10 uM of L-[^{14}C(U)]-leucine (Perkin Elmer NEC279E250UC, 11.1GBq/mMole) to CFPS reactions, followed by scintillation counting of precipitated proteins (*70*). In cases where proteins were tagged with sfGFP, reaction yields were quantified by sfGFP fluorescence. A standard curve was prepared using radioactive leucine incorporation to measure sfGFP concentration and correlate with fluorescence. To quantify sfGFP fluorescence, 2 µL of a CFPS reaction was diluted in 48 µL of water in a Black Costar 96 Well Half Area Plate. Fluorescence was measured using a BioTek Synergy™ H1 plate reader with excitation and emission wavelengths of 485 and 528 respectively. In cases where proteins were tagged with sfGFP, reaction yields were quantified by sfGFP fluorescence. A standard curve was prepared using radioactive leucine incorporation to measure sfGFP concentration and correlate with fluorescence. To quantify sfGFP fluorescence, 2 µL of a CFPS reaction was diluted in 48 µL of water in a Black Costar 96 Well Half Area Plate. Fluorescence was measured using a BioTek Synergy™ H1 plate reader with excitation and emission wavelength of 485 and 528 nm respectively.

Linear templates for Cell-Free Protein Synthesis

Plasmid constructs were amplified via PCR using the Q5 High-Fidelity DNA Polymerase and primers ACH113 (ctgagatacctacagcgtgagc) and ACH114 (cgtcactcatggtgatttctcacttg) to generate linear DNA templates for cell-free protein synthesis reactions. PCR products were purified using the Zymo Research DNA Clean & Concentrator-5 kits following the recommended protocol.

NanoBiT® reactions

NanoBiT® reactions were setup using the Promega Nano-Glo® Live Cell Assay System following the Promega NanoBiT® Technical Manual with minor modifications. Working buffer was prepared by diluting the LCS Dilution Buffer 1:4 in 1x PBS pH 7.3. CFPS reactions were diluted to the desired final concentration in working buffer and allowed to equilibrate at room temperature for the desired amount of time. The Nano-Glo® Substrate was used at a 50x final dilution of the stock. Reactions were prepared at a final volume of 2 µL, and were dispensed into 384 well plates (Nunc 267462) using the Echo® 525 liquid handler (Labcyte Inc.). Plates were immediately sealed (Bio-Rad MSB1001) and luminescence was monitored using a BioTek Synergy™ H1 plate reader.

Equilibrium logic gates were assayed by co-expressing all gate components in CFPS. Co-expressed logic gates were diluted 100-fold in working buffer and allowed to equilibrate for 72 hours before measurement. Kinetics of the induced dimerization system was measured by diluting individually expressed reaction components in working buffer to the desired level. The association reaction contained NanoBiT® fusion proteins at a final concentration of 10 nM and input protein serially diluted across a range of concentrations. Reaction luminescence was monitored

immediately after mixing components. The NOR gate input titration was set up by first diluting CFPS reactions for each component in working buffer. The mixture of NanoBiT® fusions was prepared at a concentration of 5 nM of each component. Input proteins were serially diluted in working buffer to reach the desired concentration range. Dilutions were equilibrated for 3 hours at room temperature to allow for association of the fusion proteins. Reactions were then set up by adding the appropriate volume of diluted input protein to the NanoBiT® fusion mixture. This was then allowed to equilibrate for 16 hours at room temperature before measurement. NOR gate kinetics were measured by adding 5 nM each of the NanoBiT® fusion proteins and monitoring association. After 20 minutes, 112.5 nM of ***1*** was added to the reaction and again luminescence was monitored.

T cell husbandry

CD3+ human T cells were ordered fresh from healthy donors from AllCells. Cells were activated using anti-CD3/CD28 Dynabeads from Invitrogen (Cat# 11132D). Cells were maintained in X-VIVO 15 media (Lonza, 04-418Q) with 10% FBS (HyClone Cat# SH30071), 2 mM Glutamax (Gibco Cat# 35050-061) and 1% penicillin-streptomycin (Cellgro, Cat# 30-001-CI) passed through a 0.22 um filter and supplemented with recombinant human IL-2 (Peprotech, 200-02) at a final concentration of 200U/mL. Cells were cultured in 37C w/ 5% CO_2 humidified HeraCell incubators (Thermo Scientific). Cell counts were performed by 0.4% trypan blue dye exclusion (Invitrogen, T10282).

Logic-gated control of TALE-KRAB repressors

We utilized the TALE DNA recognition domain and the KRAB repressor domain from a potent and specific synthetic transcription factor repressor targeting *TIM3* (*51*). Separated TALE DNA recognition domain and KRAB proteins each fused to obligate heterodimers using a 15 amino acid linker domain (GGGGGMDAKSLTAWS) retain activity comparable to the single chain TALE-KRAB protein when separate mRNAs encoding these molecules are electroporated into T cells (*51*). Logic gated control of TALE-KRAB repressors was engineered by pairing separated TALE and KRAB components with different orthogonal heterodimer pairs (e.g. – ***1*** of the ***1:1'*** pair). Design sequences were ordered as gBlocks from IDT and ligated into the TALE backbones.

In vitro transcription of repressors

mRNA was produced from the sequence-confirmed plasmids using the T7 mScript™ Standard mRNA Production System (CELLSCRIPT, C-MSC100625). mRNA was purified using Agencourt RNAclean XP beads (Beckman Coulter Cat#A63947), and QC of mRNA was performed on a Fragment Analyzer Infinity (Agilent) using the standard RNA kit (DNF-471-1000).

T cell electroporation

mRNA encoding TALE-TFs or heterodimeric proteins and controls were electroporated into T Cells using the BTX ECM830 Square Wave electroporator from Harvard Apparatus. Cells were collected and spun down, washed twice in PBS, and resuspended at a concentration of 250,000 cells per well in 100 ul of BTXpress high performance electroporation solution (Harvard Apparatus, Cat# 45-0805). Cells were then mixed with 1 ug of mRNA unless otherwise indicated and multichannel pipetted into MOS 96-Multi-Well Electroporation Plate_2mm (BTX, Cat# 45-0450).

Electroporation Settings: Choose Mode: LV; Set Voltage: 250 V; Set Pulse Length: 5 ms; Set Number of Pulses: 1; Electrode Type: BTX Disposable Cuvette (2mm gap); Desired Field Strength: 3000 V/cm.

Following transfection, cells were gently pipetted into warm media in a 96-well 1 mL deep well block and placed in a humidified 37°C, 5 % CO_2 incubator. GFP mRNA was always included as a control for transfection efficiency, and observed on the Cytoflex 24 hour following transfection.

T Cell flow cytometry

Cells were counted and a minimum of 100,000 cells were collected for analysis using flow cytometry on a CytoFlex S (Beckman Coulter, B75442). Cells were spun down in a 96-well V-bottom plate (Corning, 3894) and washed once in 1x PBS before staining with fluorophore-conjugated antibody diluted with 1X PBS. Staining proceeded for 30 minutes in the dark at room temperature. Following staining, cells were washed once with 1X PBS, spun down, and resuspended in 100-200 ul FACS buffer (2% heat-inactivated Fetal Bovine Serum (HyClone, SH30071.03), 1 mM EDTA (OmniPur, 4050) in 1X PBS, passed through a 0.22 um filter) for flow cytometry analysis. Antibody Brilliant Violet 421™ anti-human CD366 (Tim-3) Antibody (BioLegend, 345008) was used at a concentration of 1:50.

Progesterone-responsive yeast strain construction and growth media

The base S. cerevisiae strain used in all progesterone experiments was BY4741 (MATa his3Δ1 leu2Δ0 met15Δ0 ura3Δ0). Successive transformations of this background strain with the multi-transcriptional units encoding the fluorescence-based yeast two hybrid system (“Construction of synthetic genes”) were performed using a standard LiAc/PEG protocol (12). All yeast cultures

were grown in YPD media (10 g/L Bacto Yeast Extract, 20 g/L Bacto peptone, 20 g/L dextrose) or SDC media (6.7 g/L Bacto-yeast nitrogen base without amino acids, 2 g/L complete supplement amino acid mix, 20 g/L dextrose).

yGD390 (Fig. 1J, Fig. S4)	pHTB2s-**11'**-NLS-ZF43_8-tADH1 -- pRPL18B-**7**-NLS-VP16-tSSA1 -- pZ3-**7'-11**-NLS (SV40)-tENO1::*leu2*, pZ3-Venus-tENO2 -- p43_8(8x)-mScarlet-tPGK1::*ura3*, pPAB1-Z3PM(fixed)-tTDH1 -- pPOP6-GEM-tENO2 -- HIS3(*C. glabrata*)::*HO*

Yeast cell culture

Three colonies from the transformation of the fluorescence-based yeast two-hybrid system were used to inoculate a 1 mL YPD culture in a 2 mL 96 well storage block (Corning) to grow to saturation overnight (about 16 hours).

Progesterone induction

Saturated, overnight culture was diluted 1:500 in SDC and 450ul were aliquoted into individual wells of a new 2 mL 96 well storage block for a two hour outgrowth at 30 °C and 900 r.p.m. in a Multitron shaker (Infors HT). A Progesterone (Fisher Scientific) gradient was prepared at a 10x concentration by making the appropriate dilutions into SDC from a 3.2 mM stock solution. After the two hour outgrowth, 50ul of progesterone inducer was added to the corresponding wells of

the 96 well block and the block was returned to the shaker for six hours of post-induction growth before measurement by flow cytometry.

Yeast cell flow cytometry

Measurement of fluorescent protein reporter expression was performed with a BD LSRFortessa flow cytometer (BD Biosciences) equipped with a high-throughput sampler. After the specified induction duration, cultures were diluted 1:1 in fresh SDC for running through the high-throughput sampler, such that 3,000–10,000 events per well were collected. YFP (Venus) fluorescence was measured using the FITC channel and RFP (mScarlet) was measured using the PE-CF594 channel. Values were calculated on the height measurement and normalized to cell size by dividing by side scatter height (SSC-H). All analysis was performed in Python 3.7 using the package FlowCytometryTools and custom scripts.

Data Deposition

Raw data from native MS experiments has been deposited to http://files.ipd.uw.edu/pub/de_novo_logic_2019/190522_native_ms_raw.zip

Supplementary Text

Thermodynamic Modeling of Cooperativity

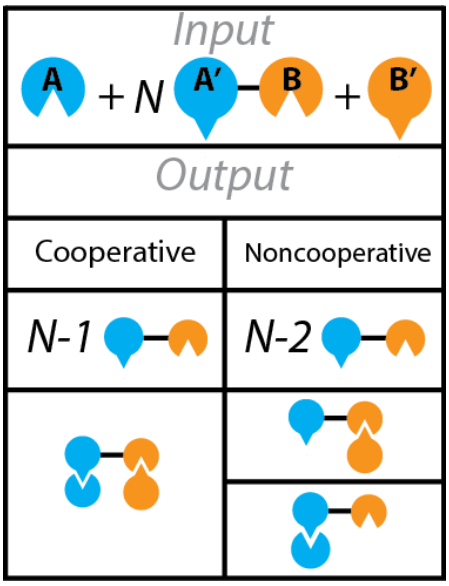

For an induced dimerization system involving proteins A, A'-B, and B', a stoichiometric excess (N>>1) of the A'-B protein results in partially assembled dimeric complexes if the binding is non-cooperative, but fully assembled trimeric complexes if the binding is cooperative.

We model the cooperatively induced dimerization system at thermodynamic equilibrium. Shown below, assuming a 'closed' state for A'-B, where the binding interfaces are buried within the four-helix bundle, the binding of A'-B to either A or B' helix hairpins needs to overcome an energy barrier of transitioning from the 'closed' to 'open' state (ΔG_{open}). Therefore the free energy of binding between A'-B to to A or B' can be expressed as $\Delta G_{A:A'}$ - ΔG_{open} and $\Delta G_{B:B'}$ - ΔG_{open}, respectively, where $\Delta G_{A:A'}$ and $\Delta G_{B:B'}$ represent the free energy of binding between the cognate pairs in the absence of the fusion. Once the A:A'-B or A-B':B complexes form, subsequent binding can simply be represented by the binding between cognate heterodimers: $\Delta G_{A:A'}$ or $\Delta G_{B:B'}$. We

also observed the presence of $(A)_2$ and $(B')_2$ homodimers, therefore we added free energy terms describing such processes into the model ($\Delta G_{A:A}$ or $\Delta G_{B':B'}$).

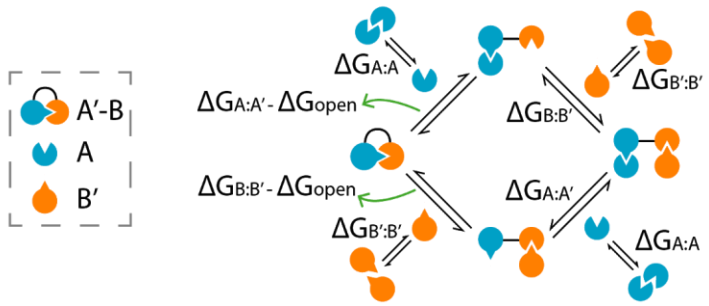

ΔG relates to equilibrium constants by $\Delta G=-RT\ln K$, and we further consider the system in terms of K. We make the simplifying assumption that the affinity of A'-B to either A or B' is identical (K_1 = [A:A'-B]/([A][A'-B]) = [A'-B:B']/([B][A'-B]). Finally, we define the cooperativity of the system, c, as the ratio between the equilibrium constants in the presence or absence of the other partner ($c=K_{B:B'}/K_1=K_{A:A'}/K_1$). For an entirely non-cooperative process (c=1), $K_{B:B'}=K_1$ and $K_{A:A'}=K_1$ *i.e.*, the first binding event does not affect the affinity of the subsequent binding event.

Since $K_1=\exp(-(\Delta G_{A:A'} - \Delta G_{open})/RT)$, rewriting the equation for c in terms of free energies leads to $c=\exp(\Delta G_{open})/RT$. Therefore, the extent of cooperativity is solely determined by the magnitude of the free energy required to partially unfold/expose the buried binding interfaces of the dimerizer A'-B.

We note that explicitly incorporating the equilibrium constants for homodimerization ($K_{A:A}$ and $K_{B':B'}$) only affect the absolute position of each equilibrium, but does not affect the magnitude of the cooperativity. Indeed, taking A as an example, the binding to the closed state becomes $K_1 * K_{A:A}$, and the binding to the open state becomes $K_{A:A'} * K_{A:A}$. Because $K_{A:A}$ is present in both the

numerator and the denominator, they cancel out, and *c* remains purely defined by the relative magnitudes of K_1 and $K_{A:A'}$.

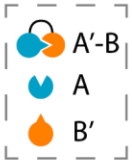

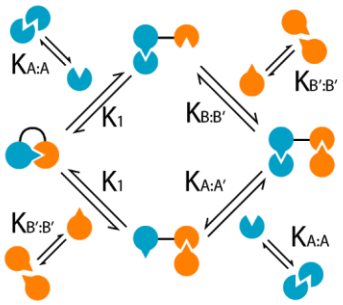

We solved the following system of equations in *Mathematica* 11 (Wolfram Research, Inc.) to simulate the amount of A:A'-B:B' at equilibrium as a function of the initial concentration of A'-B:

$$K_{A:A} = \frac{[A_2]}{[A][A]}$$

$$K_{B\prime:B\prime} = \frac{[B'_2]}{[B'][B']}$$

$$K_1 = \frac{[A:A'-B]}{[A][A'-B]}$$

$$K_1 = \frac{[B':A'-B]}{[B'][A'-B]}$$

$$K_{A:A\prime} = \frac{[A:A'-B:B']}{[A][A'-B:B']}$$

$$K_{B:B\prime} = \frac{[A:A'-B:B']}{[B'][A:A'-B]}$$

$$[A]_{tot} = 2*[A_2]+[A]+[A:A'-B]+[A:A'-B:B']$$

$$[B']_{tot} = 2*[B'_2]+[B']+[A'-B:B']+[A:A'-B:B']$$

$$[A'-B]_{tot} = [A'-B:B'] + [A:A'-B'] + [A:A'-B:B']$$

We knew from previous native MS titration experiments that the equilibrium dissociation constants of cognate designed heterodimers (DHDs) is in the ~10 nM range (*32*), therefore $K_{A:A'} = K_{B:B'} = 0.1\ nM^{-1}$. Varying values of K_1 (and hence the cooperativity factor, $c = K_{A:A'}/K_1$) showed different responses of the amount of A:A'-B:B' at equilibrium as a function of the initial concentration of A'-B, as shown in Fig. 1C.

We experimentally estimated K_1 using native MS experiments. Mixing 10 μM of ***1*** and ***1'-2'*** resulted in no detectable amount of the ***1:1'-2'*** complex, suggesting very weak binding. The sensitivity of native MS places a lower-bound on the concentration of species that can be detected (0.0375 μM, Table S8). Using this value, a lower-bound for the affinity of ***1:1'-2'*** can be estimated ($1/K_1 \geq 2.65$ mM). This agrees with the value of 9.91 mM obtained by calculating the affinity based on the *c* value of 991,000 reported in Figure 1H.

This thermodynamic modeling demonstrates that binding cooperativity can be achieved for an induced dimerization system through occlusion of the binding interfaces. We achieved this by fusing hairpins via a flexible linker, rationalizing that the spontaneous folding of these constructs would bury the interaction interfaces on the inside of a four helical bundle like topology. Formation of these structures is corroborated by: *i*) SAXS profiles that are consistent with DHDs structures, *ii*) *m*-values from chemical denaturation experiments consistent with Δ*SASA* for the unfolding of DHD topologies (Fig. S2, Table S3), and *iii*) $\Delta G_{open} < \Delta G_{folding}$, suggesting that exposing the binding interfaces requires partial unfolding of these fused constructs, but does not exceed the folding free energy of these proteins (a physically unrealistic scenario).

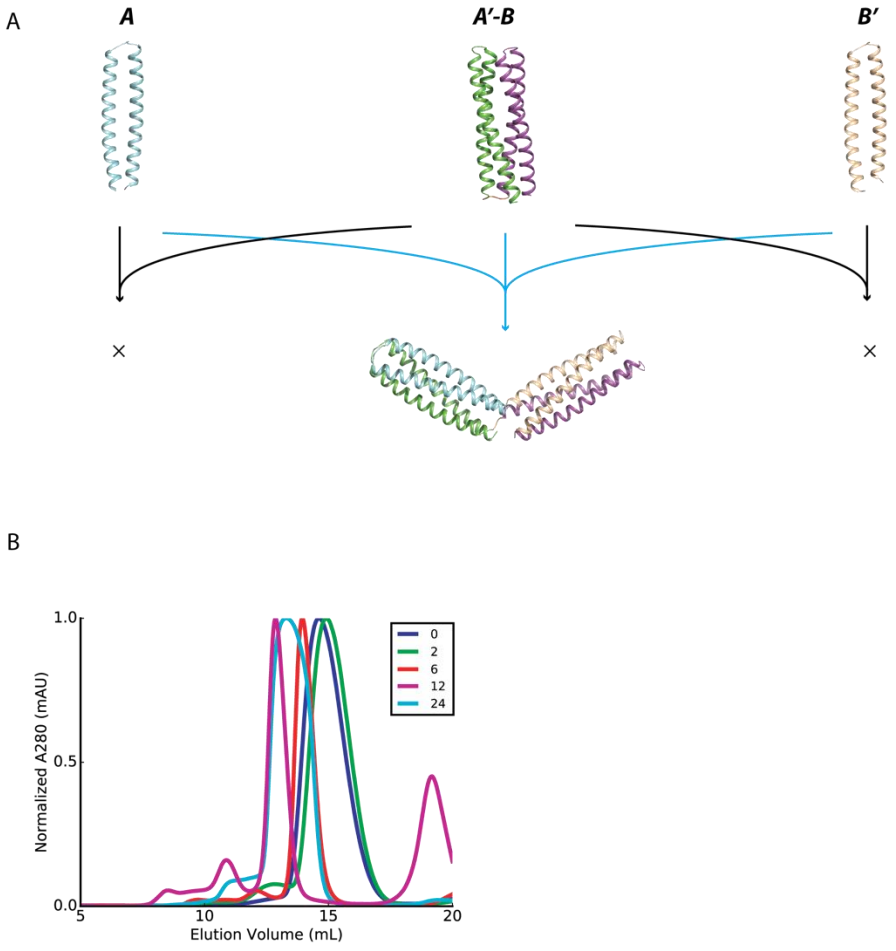

Figure S1. (A) Molecular implementation of the cooperative induced dimerization system, binding only occurs when all three components are present. **(B)** Size exclusion chromatography profiles of ***1'-2***' variants with 0, 2, 6, 12, and 24 amino acids as the flexible linker connecting ***1'*** and ***2'***.

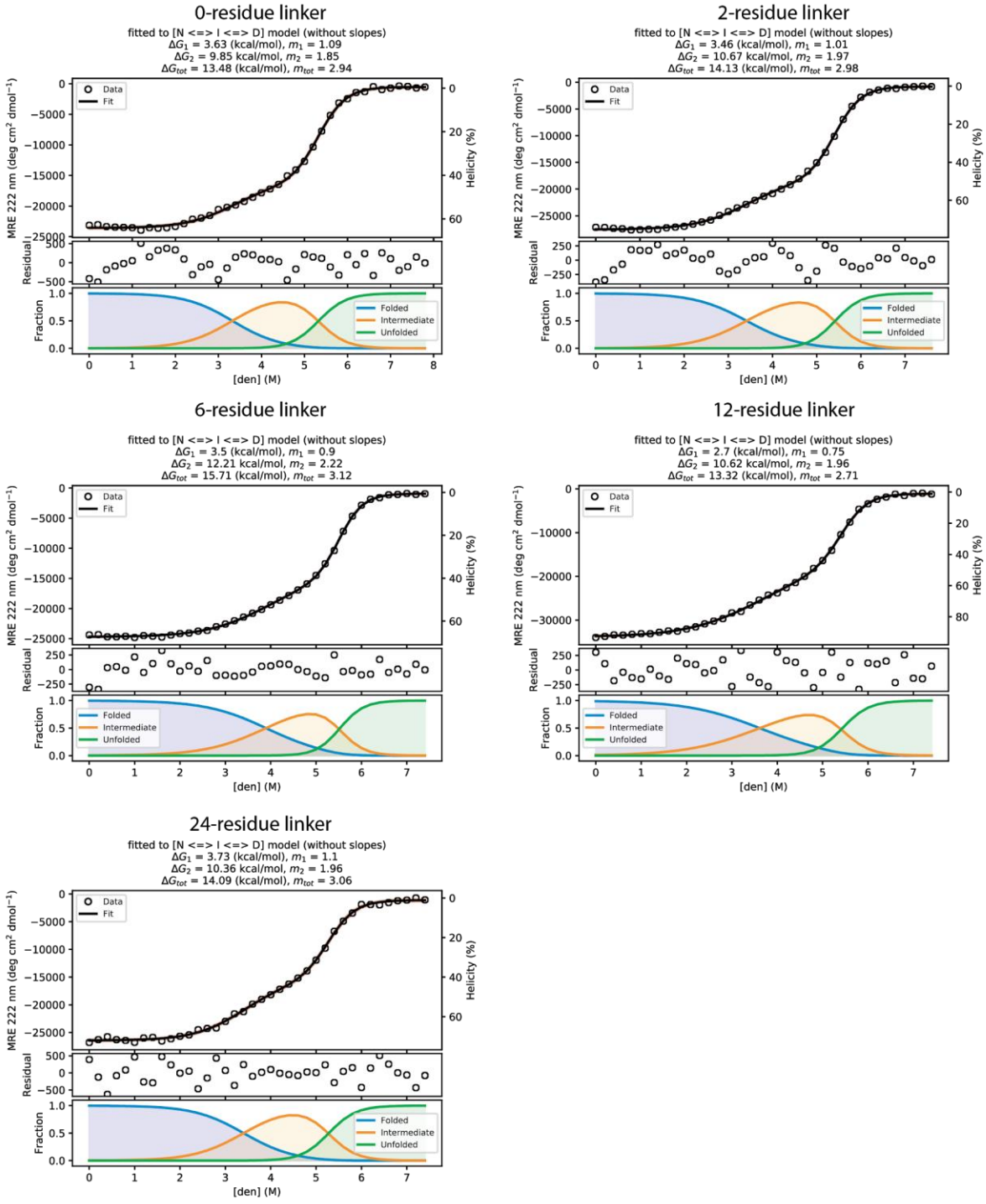

Figure S2. GdnHCl equilibrium denaturation experiments monitored by CD at 222 nm for ***1'-2'***

designs with 0-, 2-, 6-, 12- and 24- residue linkers. For each plot, the top subplot shows the experimental data (circles) fitted to the 3-state unimolecular unfolding model (black line). The middle subplots show residuals to the fit, and the bottom subplots indicate the fraction of each species as a function of denaturant concentration. An approximation of helical content is also reported (second ordinate, based on the MRE value at 222 nm using the model of Muñoz & Serrano (*71*). All fitted parameters are reported in Table S3. Δ*G* and *m*-values are also reported in the title of each plot. Δ*G* represent the free energy change extrapolated to buffer. The corresponding *m*-values represent the denaturant sensitivity of each transition, and relate to the $\Delta SASA$ associated with each event.

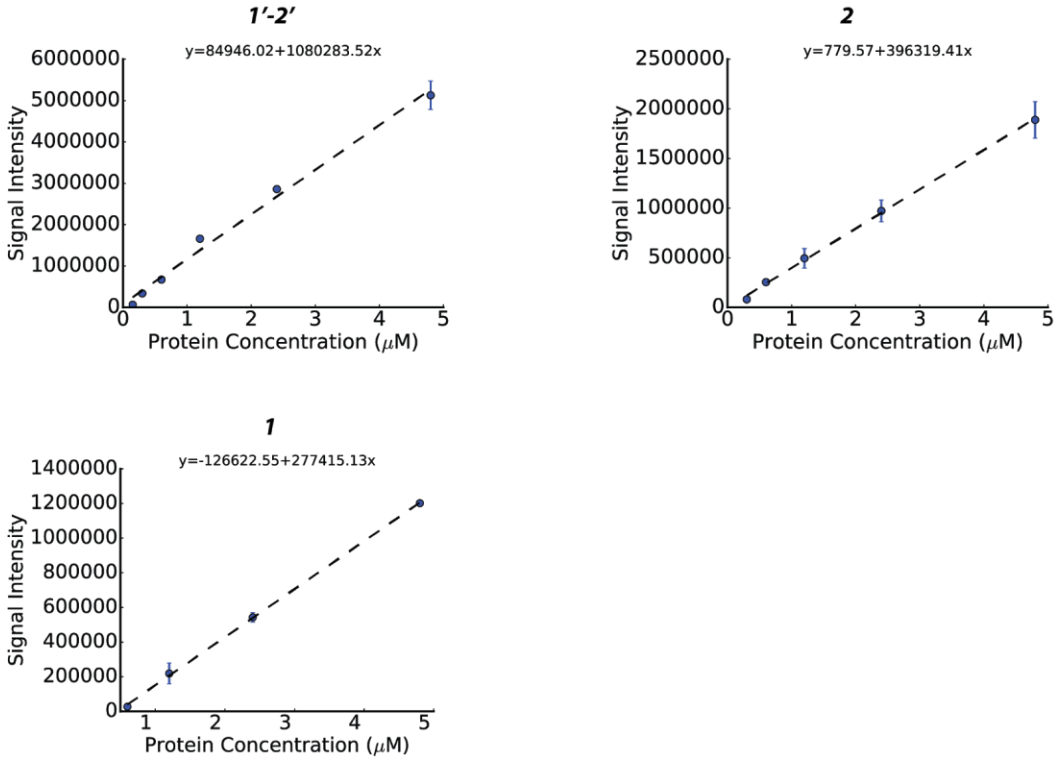

Figure S3. Native MS signal intensity of the dimerizer ***1'-2'*** (6-residue linker), ***1***, and ***2*** against protein concentrations (see also Table S8). Equations for linear regression fits are displayed. All error bars are reported as standard deviations of n=3 independent replicates.

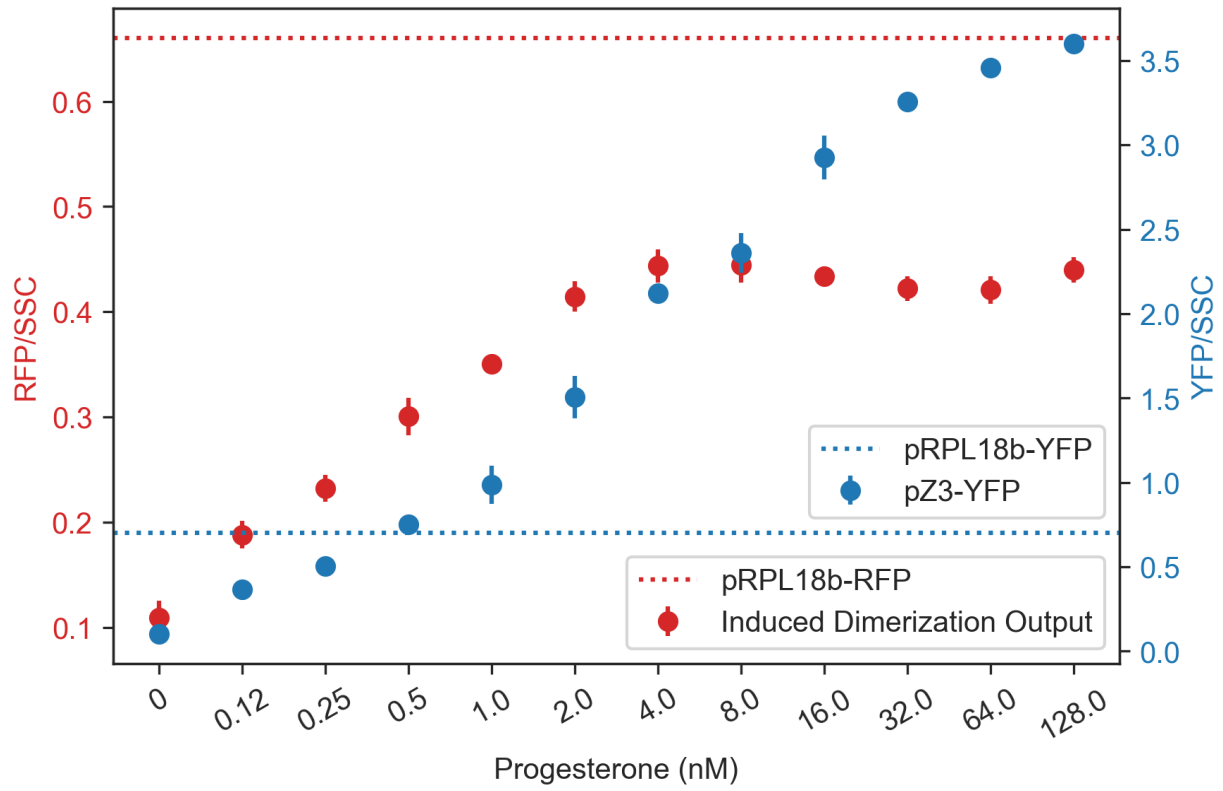

Figure S4. Induction of RFP (mScarlet) expression by the "Induced Dimerization" system in **Figure 1J**, where the dimerizer species is measured by a separate, proxy "pZ3-YFP" (Venus) reporter. Dotted lines represent constitutive expression levels of YFP and RFP under the RPL18b promoter used to express the DBD and AD monomer species in **Figure 1J**. Maximal induction of the dimerizer/YFP (128 nM Progesterone) is about 5x the value of pRPL18b-YFP, indicating that the cooperative binding functions across a wide range of concentrations. All error bars are reported as standard deviations of n=3 independent replicates.

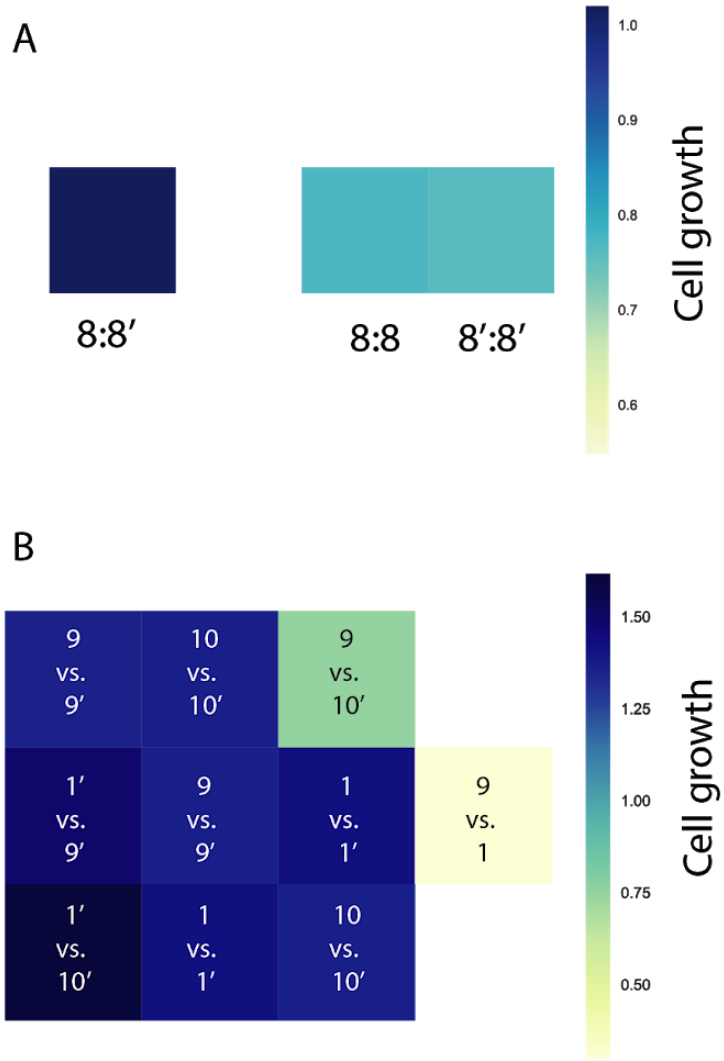

Figure S5. Binding affinity gradient from individual Y2H experiments. (A) The ***8:8′*** heterodimer binds more tightly than the homodimers of its monomers. **(B)** Binding affinity gradient among the monomers of ***1:1′***, ***9:9′***, and ***10:10′*** pairs. Cell growth was measured on different days across the rows but on the same day within each row, and not corrected against background growth.

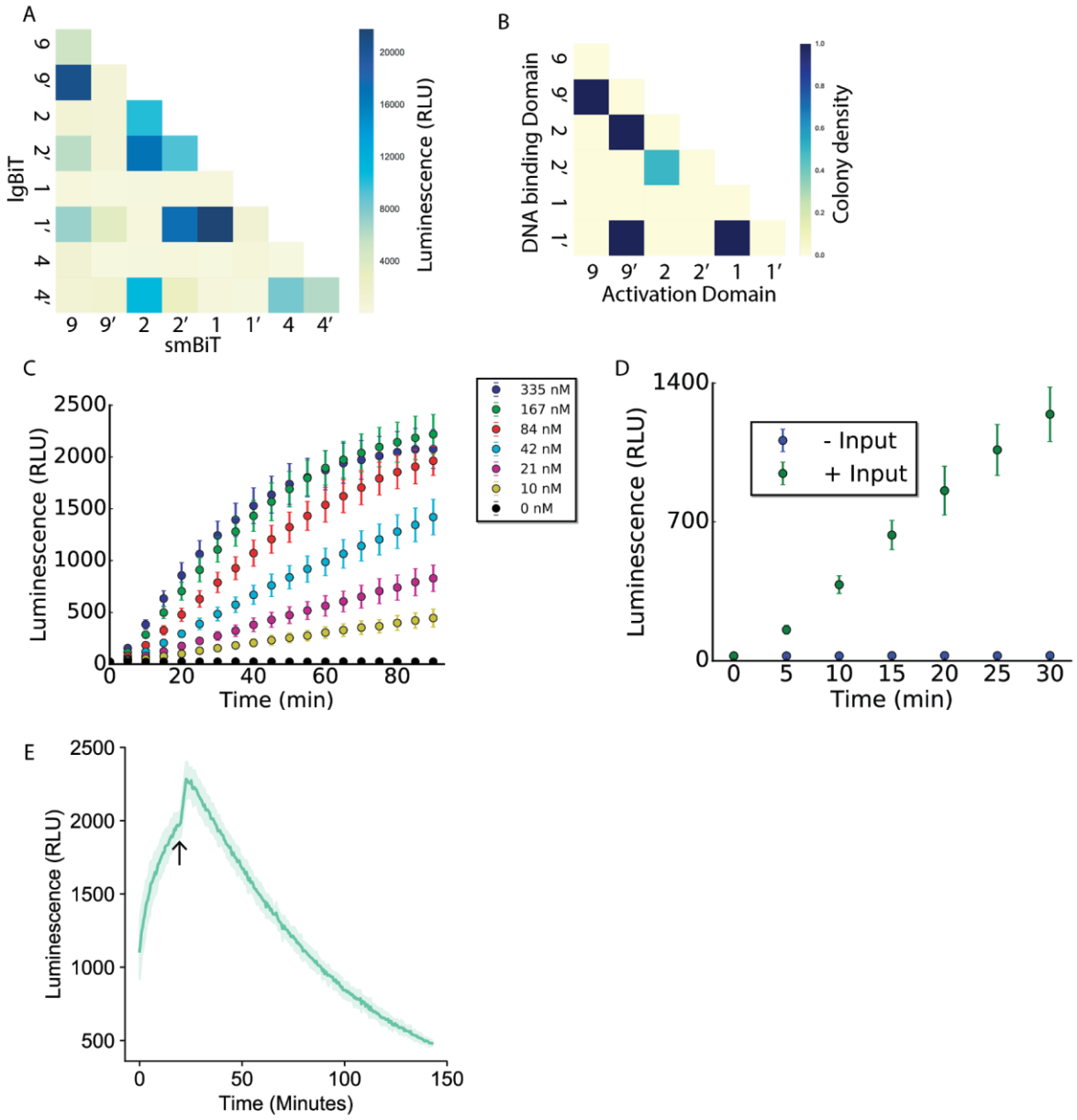

Figure S6. NanoBiT characterization of CIPHR logic gate components. (A) Specificity matrix for designs tested in the cell-free expression system. **(B)** Yeast two-hybrid specificity matrix for the same designs. **(C)** Kinetic measurements of induced dimerization gate at varying concentrations of the dimerizer input. **(D)** Kinetics of induced dimerization (with or without 335 nM dimerizer protein) in the first 30 minutes. **(E)** Kinetic measurements of NOR gate activation and

subsequent deactivation via competitive binding upon addition of input (arrow). All error bars are reported as standard deviations of n=3 independent replicates.

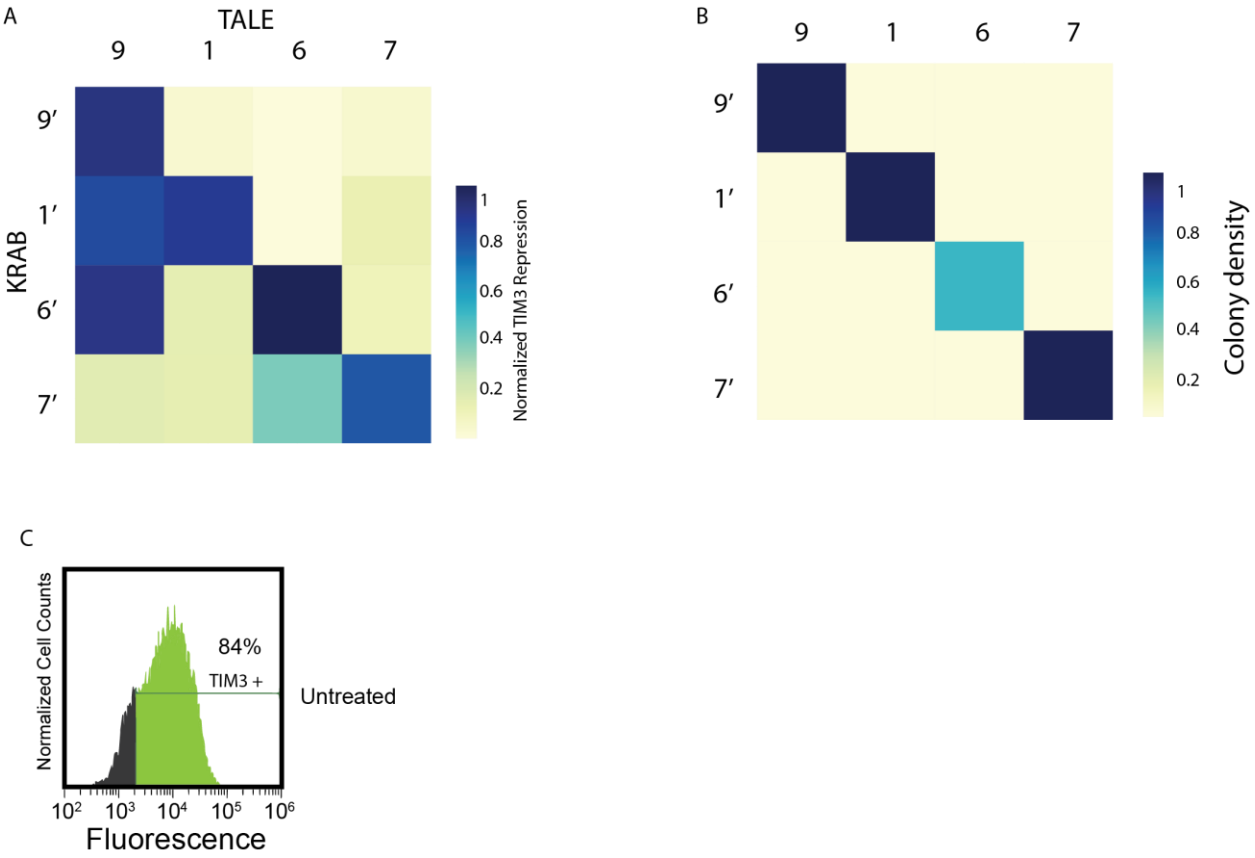

Figure S7. T cell KRAB-TALE characterization of CIPHR logic gate components. (A) Specificity matrix for designs tested in T cells. **(B)** Yeast two-hybrid specificity matrix for the same designs. **(C)** Expression level of TIM3 in T cells not treated with CIPHR logic gates.

Table S1. Design Sequences.

Amino acid sequences of all designs tested. Two versions of DHD 15 heterodimers were used here, with slight differences in the loop sequence. For simplicity they are all labeled 2 and 2', differentiated with an additional asterisk (*). See attached Supplementary Table 1.xlsx for design sequences and Vectors.zip for plasmid maps.

Table S2. SAXS analysis statistics.

Rg is the radius of gyration, Rc is the cross-sectional radius of gyration determined from Guinier fitting, and Px is the Porod exponent. The Rc value for most designs cluster around 12 Å, in a close agreement with design models.

Design name	I(0) (cm^{-1}) [Reciprocol space]	I(0) (cm-1) [Real space]	R_g [Reciprocol space]	R_g [Real space]	Porod volume estimate (10,000 $Å^3$)	Dmax (Å)	R_c (Å)	P_x
15B-37B_linker6	13.00	12.00	21.54	21.06	4.2	63	12.46	3
15B-37B_linker12	13.00	12.00	20.86	20.66	3.9	62	12.04	3
15A	17.00	17.00	19.22	19.86	3.5	61	12.58	3.4
37A	17.00	14.00	22.51	21.43	4.5	65	13.3	3.1
15B-131A	8.30	7.60	20.67	20.91	4.1	65	12.26	2.8
131B-37B	12.00	9.90	28.82	27.31	7.3	85	15.14	2.8
131B-101A	12.00	11.00	21.14	21.35	4.4	65	13.72	3.1

Table S3. CD data parameter fitting.

Fitted parameters for equilibrium chemical denaturation. Errors represent fitting errors.

	Linker 0	**Linker 2**	**Linker 6**	**Linker 12**	**Linker 24**
$\Delta G_1^{(N \Leftrightarrow I)}$ (kcal mol^{-1})	3.6 (±0.4)	3.5 (±0.2)	3.5 (±0.2)	2.7 (±0.1)	3.7 (±0.3)
$\Delta G_2^{(I \Leftrightarrow D)}$ (kcal mol^{-1})	9.8 (±0.6)	10.7 (±0.4)	12.2 (±0.4)	10.6 (±0.5)	10.4 (±0.8)
$\Delta G_{tot}^{(N \Leftrightarrow D)}$ (kcal mol^{-1})	13.5 (±0.7)	14.1 (±0.4)	15.7 (±0.5)	13.3 (±0.5)	14.1 (±0.8)
m_1 (kcal mol^{-1} M^{-1})	1.1 (±0.2)	1.0 (±0.1)	0.9 (±0.1)	0.75 (±0.05)	1.1 (±0.1)
m_2 (kcal mol^{-1} M^{-1})	1.8 (±0.1)	1.97 (±0.07)	2.22 (±0.08)	1.96 (±0.08)	2.0 (±0.1)
m_{tot} (kcal mol^{-1} M^{-1})	2.9 (±0.2)	3.0 (±0.1)	3.1 (±0.1)	2.71 (±0.09)	3.1 (±0.2)
MRE_N (deg cm^2 dmol^{-1})	-23,574 (±114)	-27,561 (±84)	-24,712 (±63)	-33,849 (±131)	-26,438 (±123)
MRE_I (deg cm^2 dmol^{-1})	-16,330 (±749)	-18,139 (±540)	-14,779 (±710)	-17,362 (±1,158)	-15,567 (±914)
MRE_D (deg cm^2 dmol^{-1})	-525 (±107)	-785 (±82)	-937 (±68)	-1,104 (±99)	-1,125 (±133)

Table S4. Native MS spectra of individual designs.

5 µL protein (10-100 pmol) were injected and detected by online buffer exchange coupled to an Exactive Plus EMR Orbitrap instrument. Spectra were deconvoluted by UniDec. Species and determined molecular weights are depicted. Signals corresponding to monomers are indicated by an orange circle, dimers are indicated by a red square.

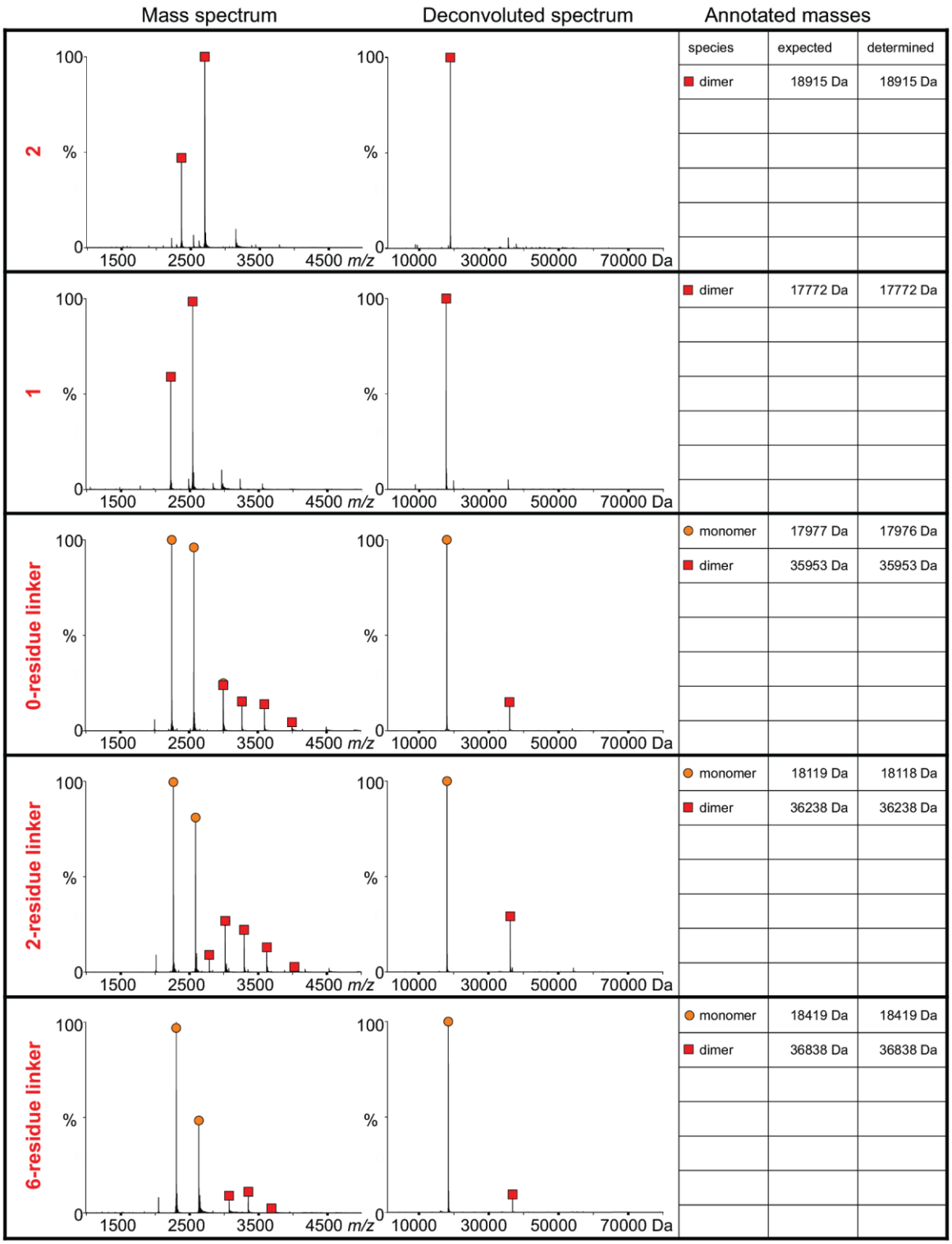
Mass spectrum
Deconvoluted spectrum
Annotated masses
2
1
0-residue linker
2-residue linker
6-residue linker
100
%
0
1500
2500
3500
4500 m/z
10000
30000
50000
70000 Da
species
expected
determined
dimer
18915 Da
18915 Da
dimer
17772 Da
17772 Da
monomer
17977 Da
17976 Da
dimer
35953 Da
35953 Da
monomer
18119 Da
18118 Da
dimer
36238 Da
36238 Da
monomer
18419 Da
18419 Da
dimer
36838 Da
36838 Da

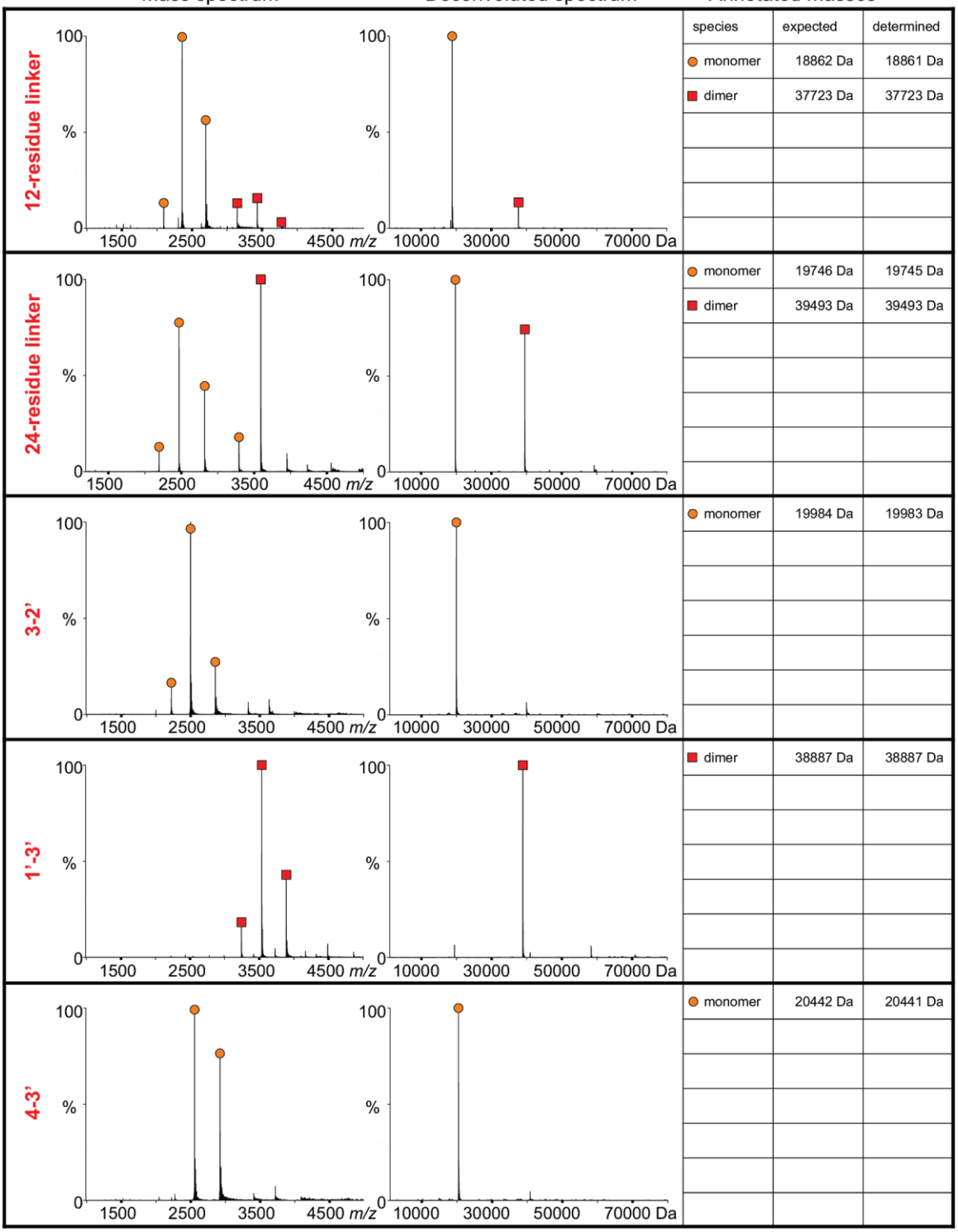

species	expected	determined
12-residue linker		
monomer	18862 Da	18861 Da
dimer	37723 Da	37723 Da
24-residue linker		
monomer	19746 Da	19745 Da
dimer	39493 Da	39493 Da
3-2'		
monomer	19984 Da	19983 Da
1'-3'		
dimer	38887 Da	38887 Da
4-3'		
monomer	20442 Da	20441 Da

Mass spectrum

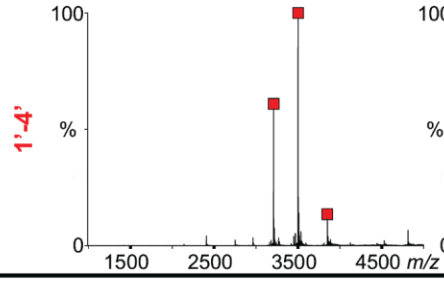

Deconvoluted spectrum

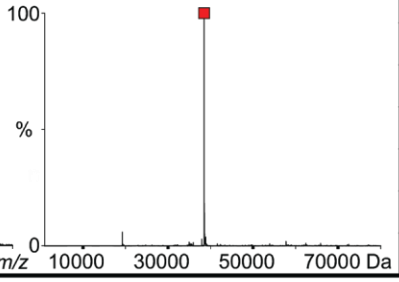

Annotated masses

species	expected	determined
dimer	38497 Da	38497 Da

Table S5. Protein concentrations native MS titration experiments.

Titration for Figure 1G						
Design	concentration/ µM					
2	0	3	6	10	15	20
1	10	10	10	10	10	10
1'-2'	10	10	10	10	10	10

Titration for Figure 1H								
Design	concentration/ µM							
2	10	10	10	10	10	10	10	10
1	10	10	10	10	10	10	10	10
1'-2'	0	3	6	10	15	20	40	60

Titration for Figure 1L								
Design	concentration/ µM							
2	10	10	10	10	10	10	10	10
1	10	10	10	10	10	10	10	10
3-2'	0	3	6	10	15	20	40	60
1'-3'	0	3	6	10	15	20	40	60

Titration for Figure 1N								
Design	concentration/ µM							
2	10	10	10	10	10	10	10	10
1	10	10	10	10	10	10	10	10
1'-4'	0	3	6	10	15	20	40	60
4-3'	0	3	6	10	15	20	40	60
3-2'	0	3	6	10	15	20	40	60

Table S6. Native MS spectra of complexes.

Samples were prepared by mixing equimolar amounts of ***1***, ***2***, and the corresponding dimerizer(s) (i.e.***1'-2'*** for induced dimerization, ***1'-3'*** + ***3-2'*** for 2-in AND, linker ***1'-4***+ ***4-3'***+ ***3-2'***+ for 3-in AND). After denaturation, refolding and dialysis against 200 mM AmAc, the mixtures were diluted 12.5 fold with 200 mM AmAc and 5 µL were flow-injected into an Exactive Plus EMR Orbitrap instrument. Spectra were deconvoluted by UniDec. Species and determined molecular weights are depicted. Signals corresponding to the 1-(dimerizer)n-2 complex are indicated by a red circle, free dimerizer is indicated by a yellow star.

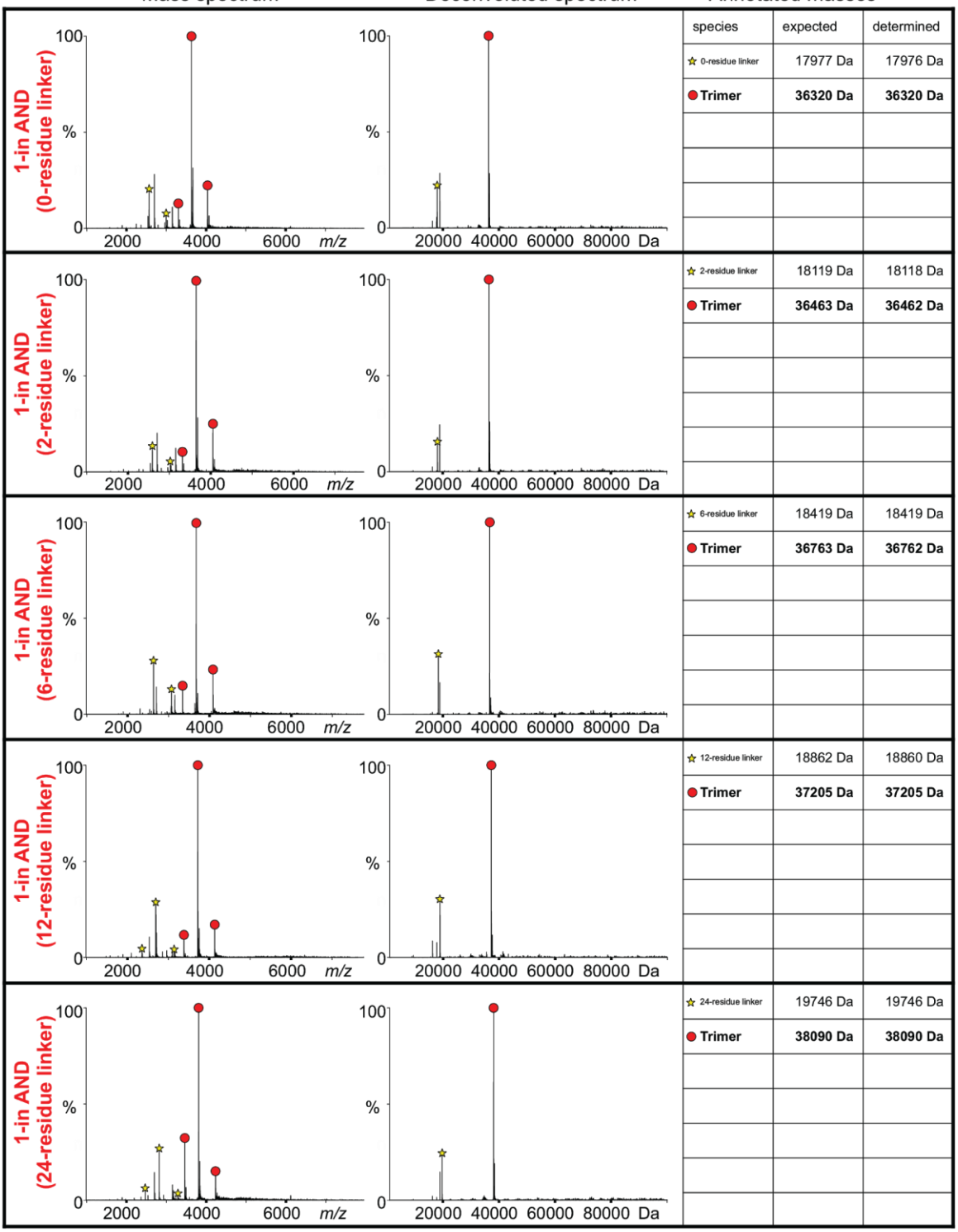
Mass spectrum
Deconvoluted spectrum
Annotated masses
1-in AND (0-residue linker)
1-in AND (2-residue linker)
1-in AND (6-residue linker)
1-in AND (12-residue linker)
1-in AND (24-residue linker)
100
%
0
2000
4000
6000
m/z
20000
40000
60000
80000
Da
species
expected
determined
0-residue linker
17977 Da
17976 Da
Trimer
36320 Da
36320 Da
2-residue linker
18119 Da
18118 Da
Trimer
36463 Da
36462 Da
6-residue linker
18419 Da
18419 Da
Trimer
36763 Da
36762 Da
12-residue linker
18862 Da
18860 Da
Trimer
37205 Da
37205 Da
24-residue linker
19746 Da
19746 Da
Trimer
38090 Da
38090 Da

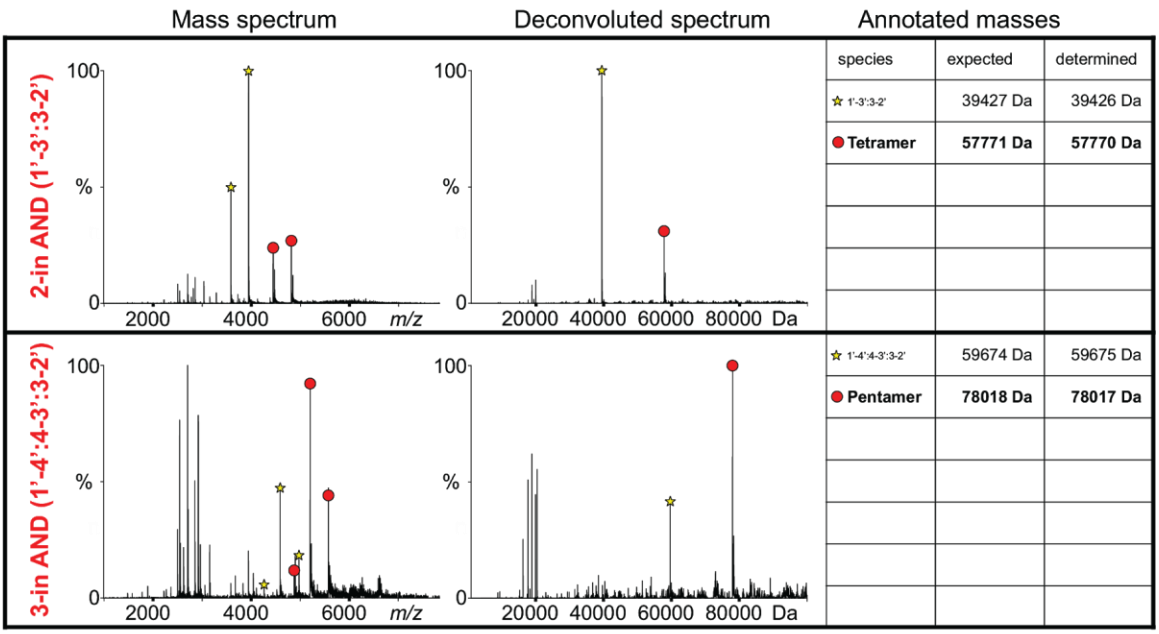
Mass spectrum
Deconvoluted spectrum
Annotated masses
2-in AND (1'-3':3-2')
3-in AND (1'-4':4-3':3-2')
100
%
0
2000
4000
6000
m/z
20000
40000
60000
80000
Da
species
expected
determined
1'-3':3-2'
39427 Da
39426 Da
Tetramer
57771 Da
57770 Da
1'-4':4-3':3-2'
59674 Da
59675 Da
Pentamer
78018 Da
78017 Da

Table S7. Detailed native MS titration spectra of AND logic gates.

Samples were prepared by mixing 10 µM ***1*** and ***2*** with 0 – 60 µM of (A) ***1'-2'*** with 0-residue linker, (B) ***1'-2'*** with 2-residue linker, (C) ***1'-2'*** with 6-residue linker, (D) ***1'-2'*** with 12-residue linker, (E) ***1'-2'*** with 24-residue linker, (F) ***1'-3'*** + ***3-2'***, and (G) ***1'-4***+ ***4-3'***+ ***3-2'***. After denaturation, refolding and dialysis against 200 mM AmAc, the mixtures were diluted 12.5 fold with 200 mM AmAc and 5 µL were flow-injected into an Exactive Plus EMR Orbitrap instrument. Signals corresponding to the full trimer complexes in (A) - (E), full tetramer complex in (F) and full pentamer complex in (G) are indicated by a red circle. Free dimerizer/ dimerizer complexes are indicated by a blue triangle. The spectra for each titration were normalized and stacked to visualize the change in complex abundance in dependency of added dimerizer(s). As indicated by a red arrow and dashed line, in (G) relative intensities for signals with *m/z* >4300 are magnified 4x, and in (E) relative intensities for signals with *m/z* >4200 are magnified 5x for *m/z* >4200 to help visualize formation of full complexes in the presence of the easily ionizable dimerizers. Lists of all identified and quantified species in the titration has been deposited.

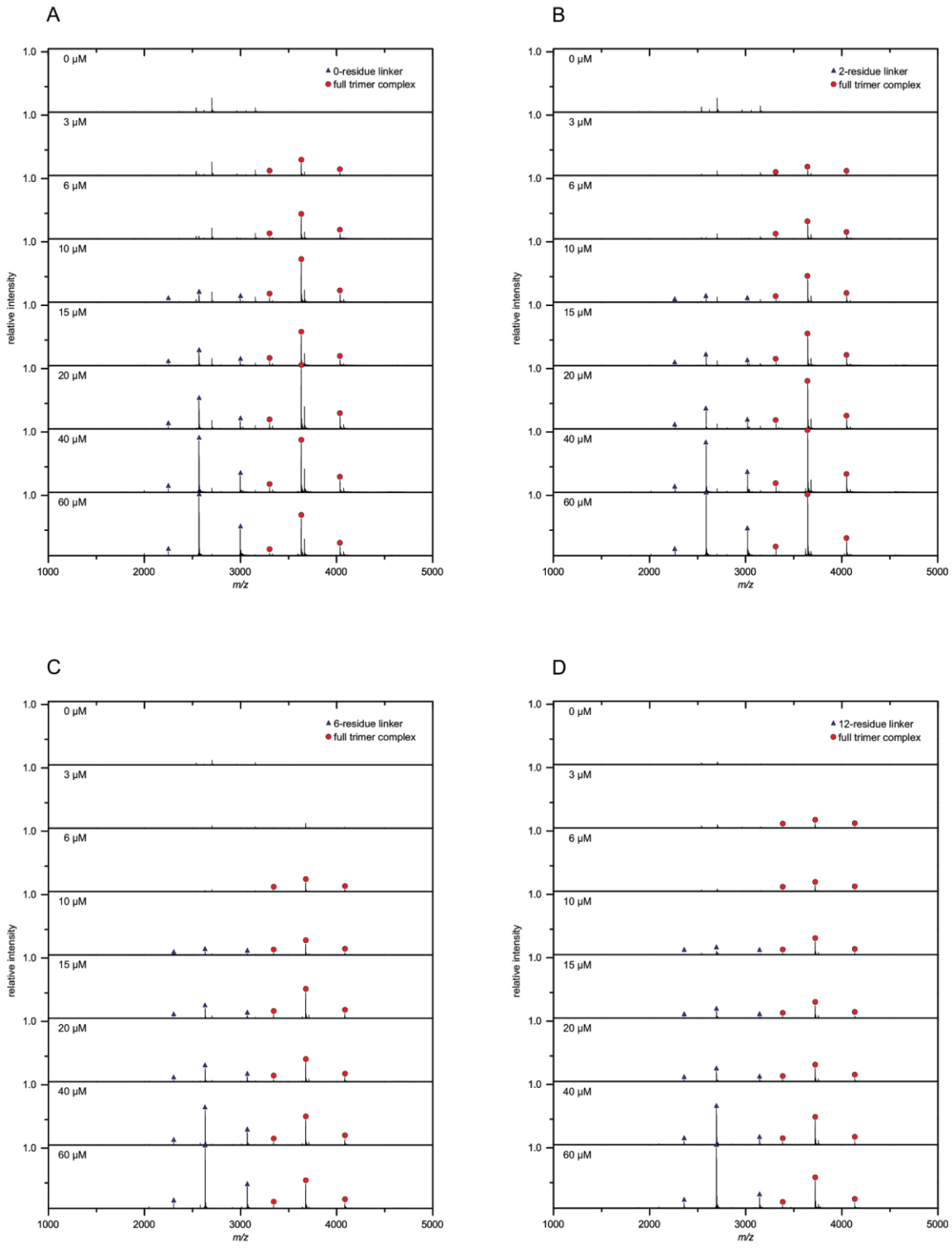
A
B
C
D
0 μM
3 μM
6 μM
10 μM
15 μM
20 μM
40 μM
60 μM
0-residue linker
2-residue linker
6-residue linker
12-residue linker
full trimer complex
relative intensity
m/z
1000
2000
3000
4000
5000
1.0

E

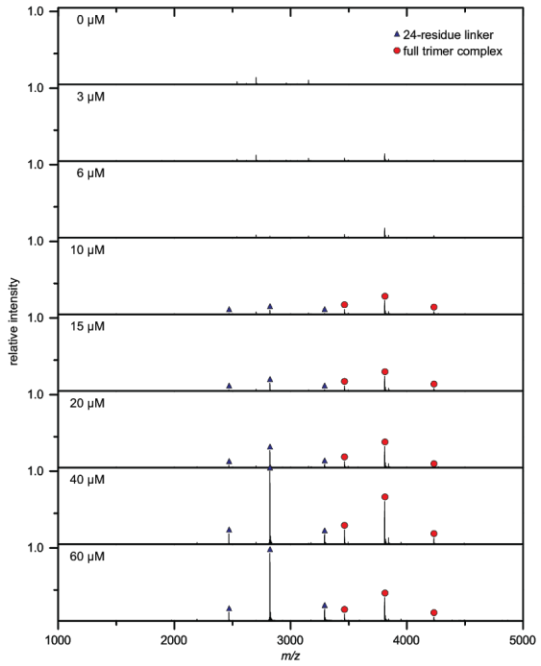
0 μM
3 μM
6 μM
10 μM
15 μM
20 μM
40 μM
60 μM
24-residue linker
full trimer complex
relative intensity
m/z
1000
2000
3000
4000
5000

F

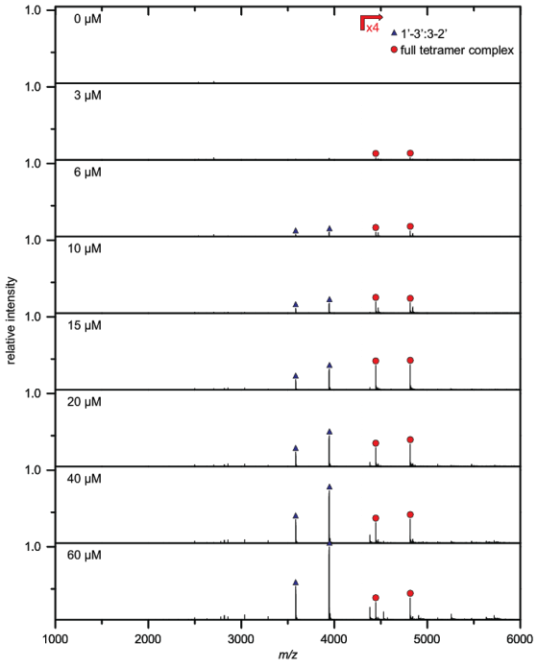
0 μM
3 μM
6 μM
10 μM
15 μM
20 μM
40 μM
60 μM
x4
1'-3':3-2'
full tetramer complex
relative intensity
m/z
1000
2000
3000
4000
5000
6000

G

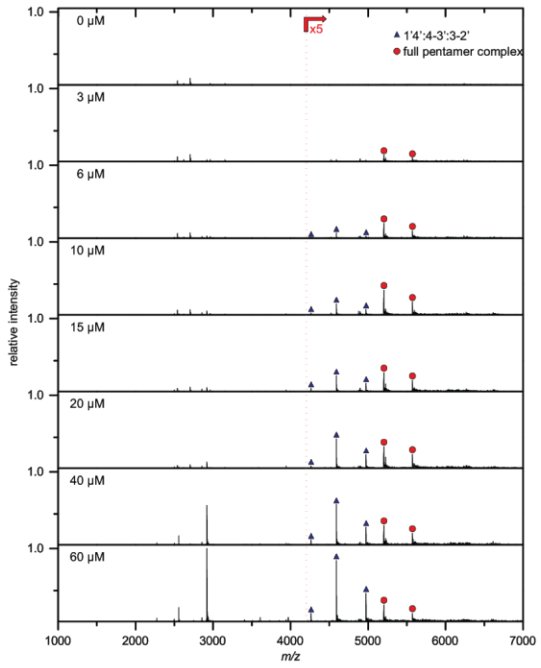
0 μM
3 μM
6 μM
10 μM
15 μM
20 μM
40 μM
60 μM
x5
1'4':4-3':3-2'
full pentamer complex
relative intensity
m/z
1000
2000
3000
4000
5000
6000
7000

Table S8. Native MS spectra of serial dilution experiments.

Samples at 60 µM monomer concentration were prepared by denaturation, refolding and dialysis against 200 mM AmAc. Proteins were diluted to the indicated concentrations (4.8 µM to 0.0375 µM). 5 µL (24 pmole to 0.1875 pmole) were flow-injected into an Exactive Plus EMR Orbitrap instrument. Spectra were deconvoluted by UniDec. Species and determined molecular weights are depicted. Signals corresponding to monomers are indicated by an orange circle, dimers are indicated by a red square. Total ion chromatograms (1000-8000 *m/z*) are depicted for flow-injection profiles.

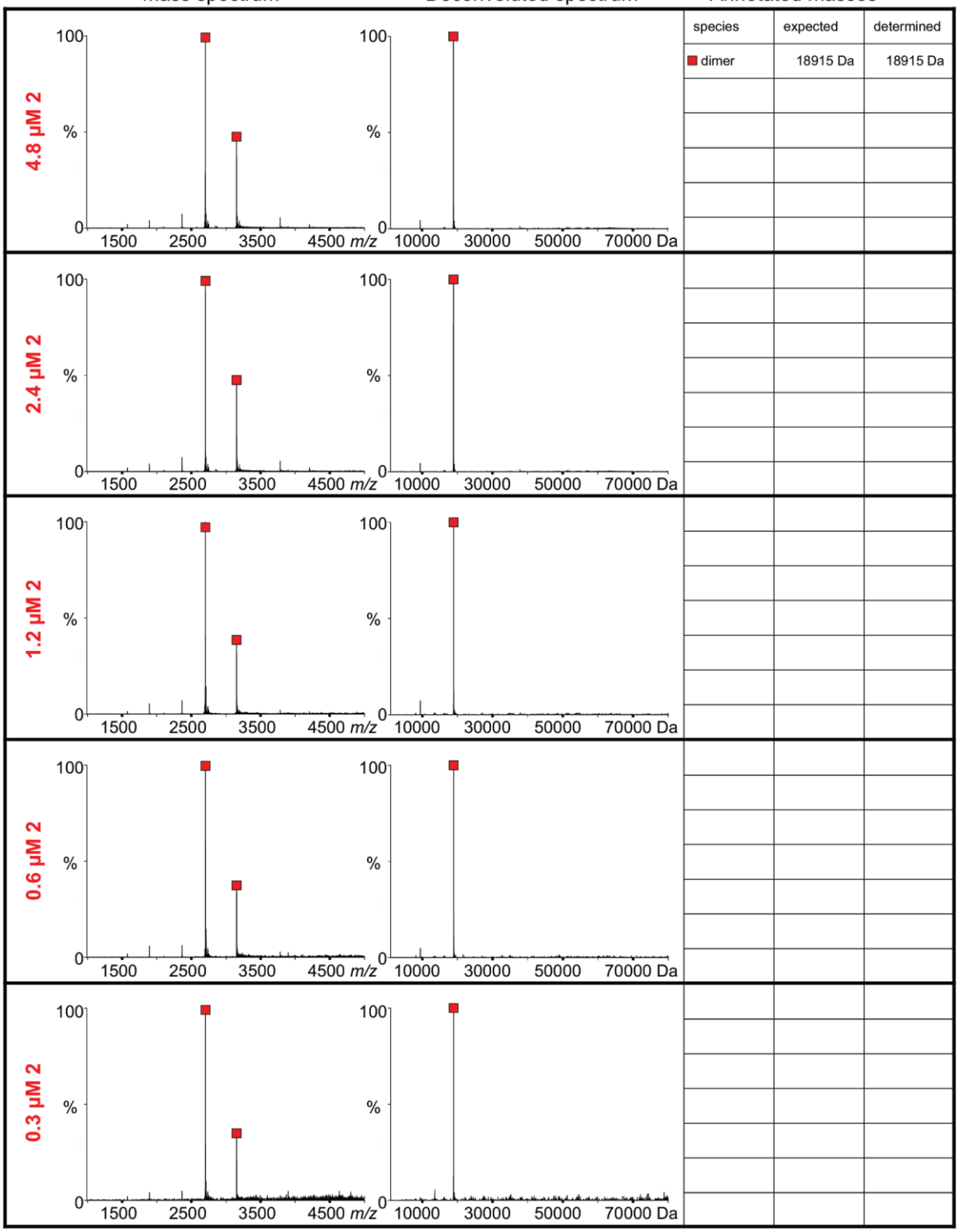
Mass spectrum
Deconvoluted spectrum
Annotated masses
species
expected
determined
dimer
18915 Da
18915 Da
4.8 µM 2
2.4 µM 2
1.2 µM 2
0.6 µM 2
0.3 µM 2
100
%
0
1500
2500
3500
4500 m/z
10000
30000
50000
70000 Da

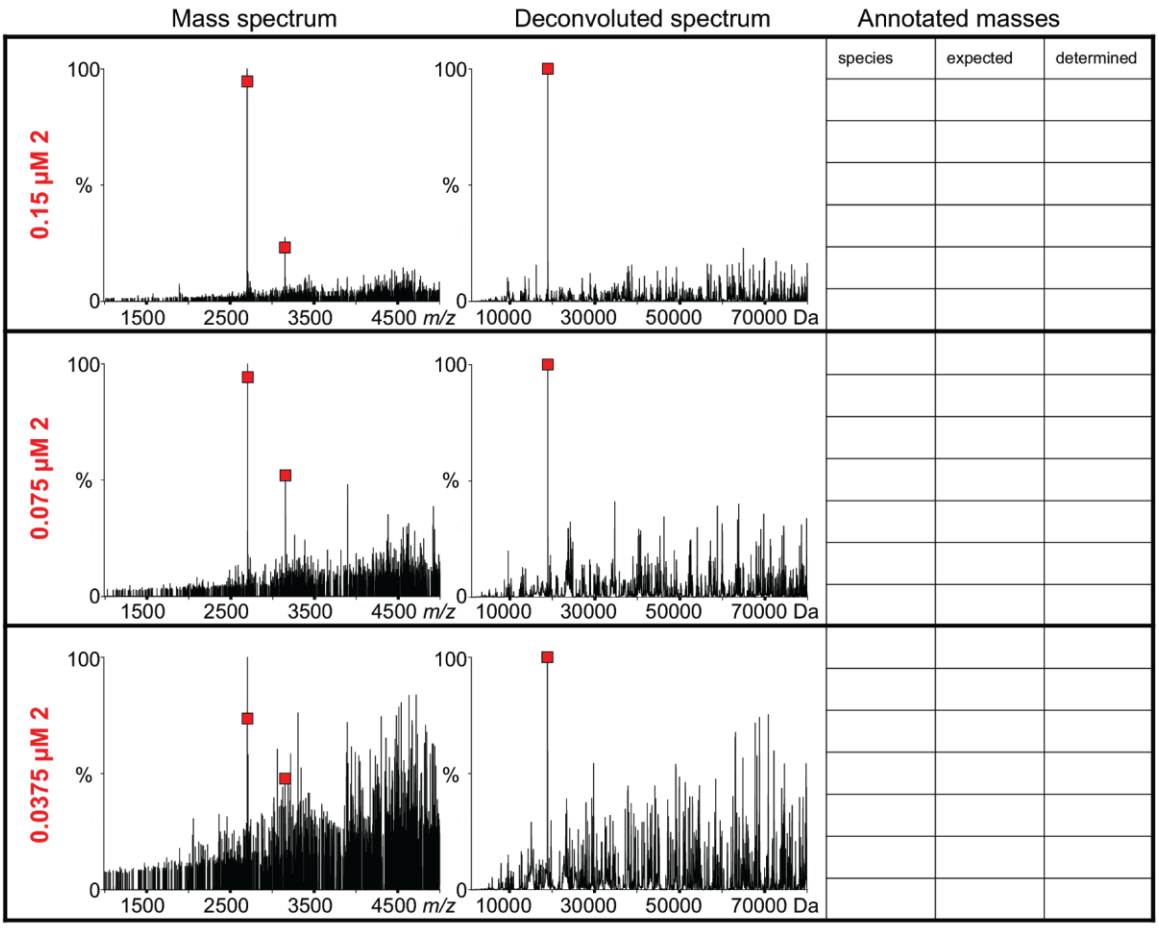
Mass spectrum
Deconvoluted spectrum
Annotated masses
species
expected
determined
0.15 µM 2
0.075 µM 2
0.0375 µM 2
100
%
0
1500
2500
3500
4500 m/z
10000
30000
50000
70000 Da

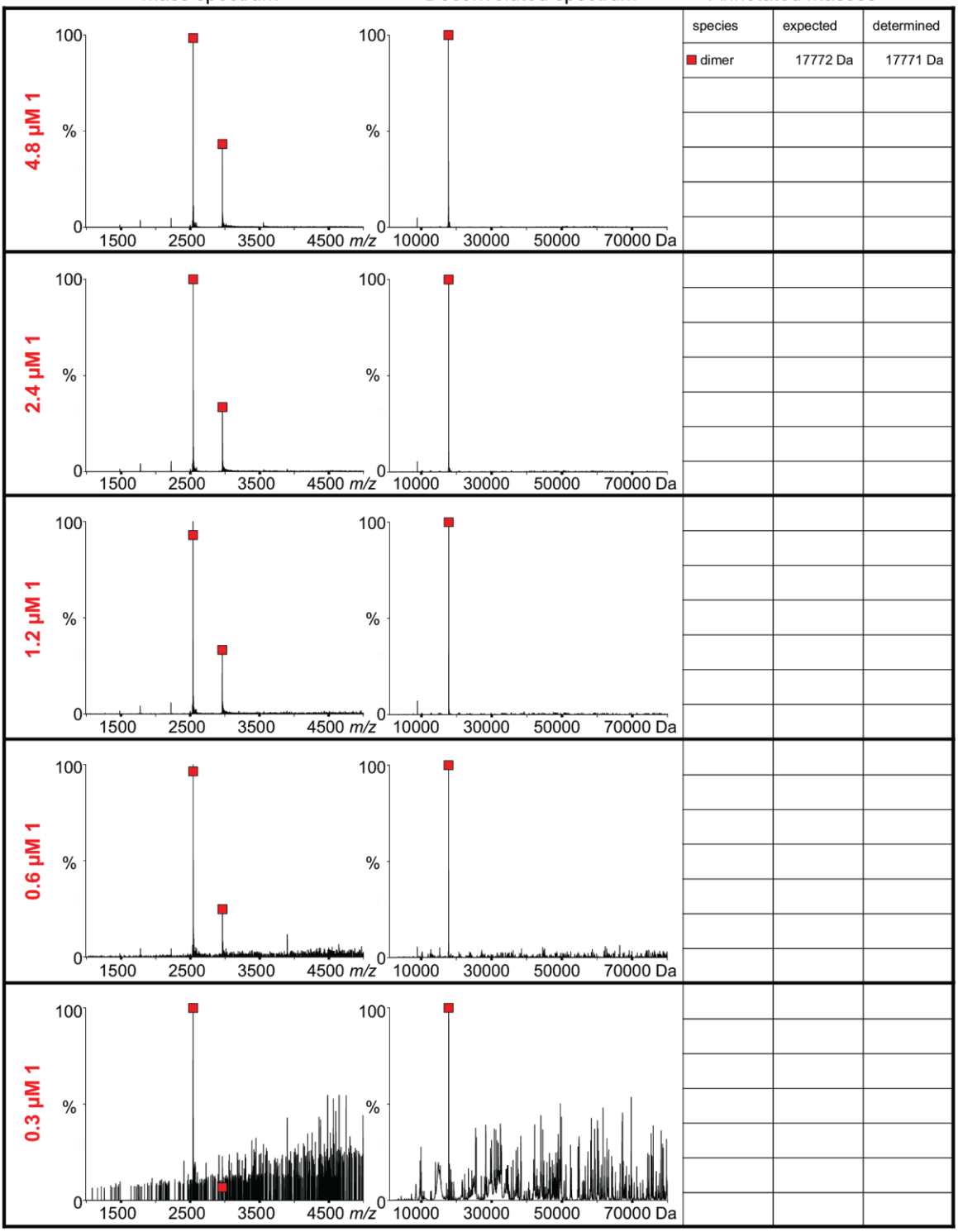
Mass spectrum
Deconvoluted spectrum
Annotated masses
4.8 µM 1
2.4 µM 1
1.2 µM 1
0.6 µM 1
0.3 µM 1
100
%
0
1500
2500
3500
4500 m/z
10000
30000
50000
70000 Da
species
expected
determined
dimer
17772 Da
17771 Da

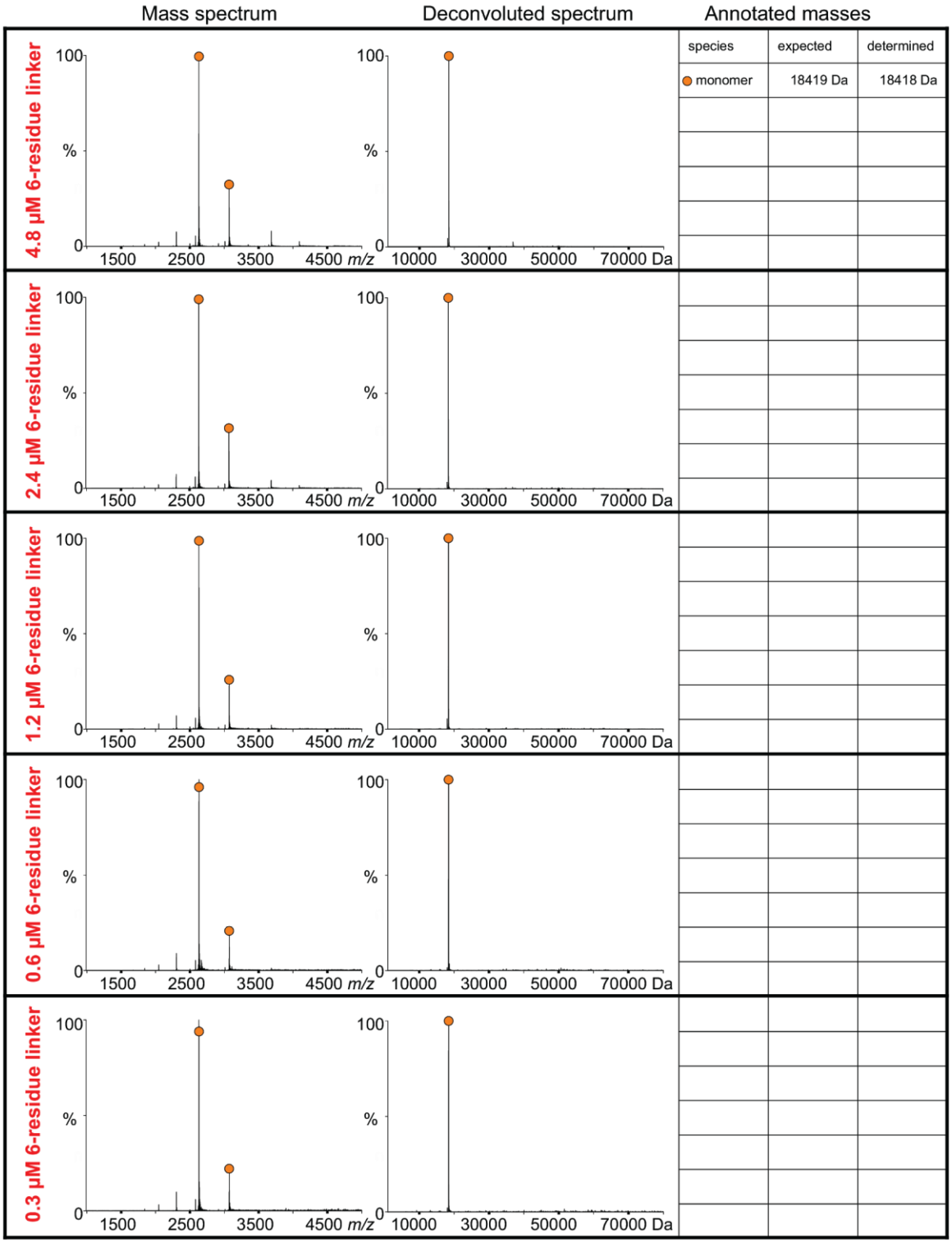
Mass spectrum
Deconvoluted spectrum
Annotated masses
4.8 µM 6-residue linker
2.4 µM 6-residue linker
1.2 µM 6-residue linker
0.6 µM 6-residue linker
0.3 µM 6-residue linker
100
%
0
1500
2500
3500
4500 m/z
10000
30000
50000
70000 Da
species
expected
determined
monomer
18419 Da
18418 Da

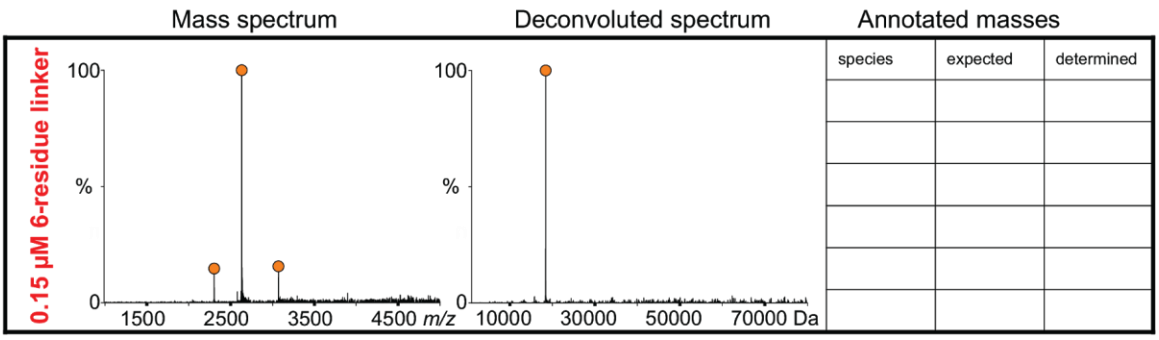
Mass spectrum
Deconvoluted spectrum
Annotated masses
0.15 µM 6-residue linker
100
%
0
1500
2500
3500
4500 m/z
10000
30000
50000
70000 Da
species
expected
determined

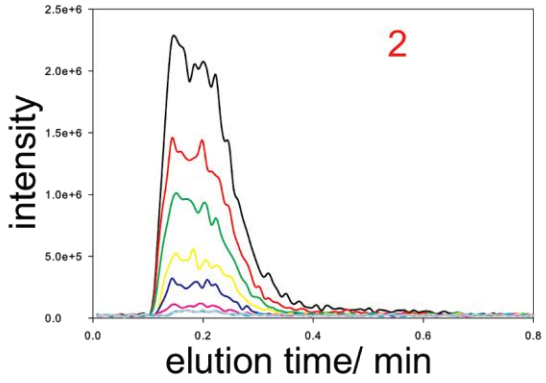
2
intensity
elution time/ min

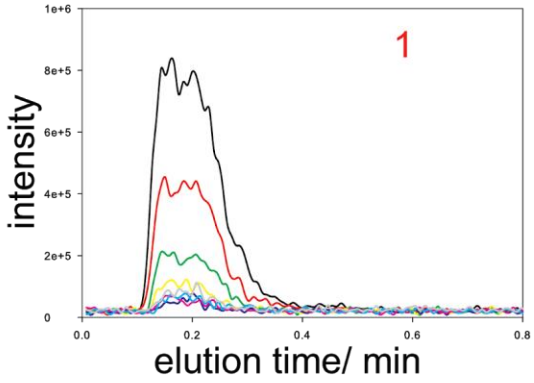
1
intensity
elution time/ min

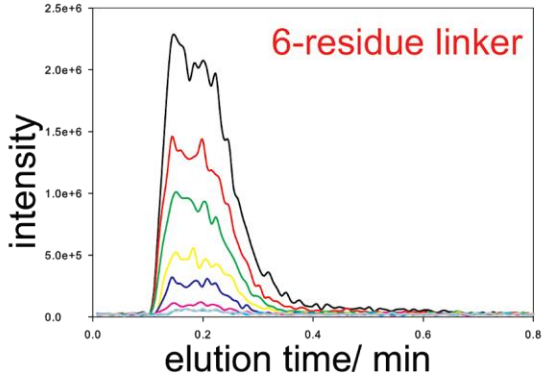
6-residue linker
intensity
elution time/ min

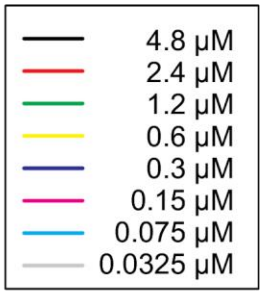
4.8 µM
2.4 µM
1.2 µM
0.6 µM
0.3 µM
0.15 µM
0.075 µM
0.0325 µM

References and Notes

1. R. Nussinov, How do dynamic cellular signals travel long distances? *Mol. Biosyst.* **8**, 22–26 (2012). doi:10.1039/C1MB05205E Medline

2. A. W. Reinke, J. Baek, O. Ashenberg, A. E. Keating, Networks of bZIP protein-protein interactions diversified over a billion years of evolution. *Science* **340**, 730–734 (2013). doi:10.1126/science.1233465 Medline

3. Y. E. Antebi, J. M. Linton, H. Klumpe, B. Bintu, M. Gong, C. Su, R. McCardell, M. B. Elowitz, Combinatorial signal perception in the BMP pathway. *Cell* **170**, 1184–1196.e24 (2017). doi:10.1016/j.cell.2017.08.015 Medline

4. B. Z. Harris, W. A. Lim, Mechanism and role of PDZ domains in signaling complex assembly. *J. Cell Sci.* **114**, 3219–3231 (2001). Medline

5. G. Seelig, D. Soloveichik, D. Y. Zhang, E. Winfree, Enzyme-free nucleic acid logic circuits. *Science* **314**, 1585–1588 (2006). doi:10.1126/science.1132493 Medline

6. L. Qian, E. Winfree, Scaling up digital circuit computation with DNA strand displacement cascades. *Science* **332**, 1196–1201 (2011). doi:10.1126/science.1200520 Medline

7. M. B. Elowitz, S. Leibler, A synthetic oscillatory network of transcriptional regulators. *Nature* **403**, 335–338 (2000). doi:10.1038/35002125 Medline

8. T. S. Gardner, C. R. Cantor, J. J. Collins, Construction of a genetic toggle switch in Escherichia coli. *Nature* **403**, 339–342 (2000). doi:10.1038/35002131 Medline

9. A. Tamsir, J. J. Tabor, C. A. Voigt, Robust multicellular computing using genetically encoded NOR gates and chemical ‘wires’. *Nature* **469**, 212–215 (2011). doi:10.1038/nature09565 Medline

10. P. Siuti, J. Yazbek, T. K. Lu, Synthetic circuits integrating logic and memory in living cells. *Nat. Biotechnol.* **31**, 448–452 (2013). doi:10.1038/nbt.2510 Medline

11. J. Bonnet, P. Yin, M. E. Ortiz, P. Subsoontorn, D. Endy, Amplifying genetic logic gates. *Science* **340**, 599–603 (2013). doi:10.1126/science.1232758 Medline

12. B. H. Weinberg, N. T. H. Pham, L. D. Caraballo, T. Lozanoski, A. Engel, S. Bhatia, W. W. Wong, Large-scale design of robust genetic circuits with multiple inputs and outputs for mammalian cells. *Nat. Biotechnol.* **35**, 453–462 (2017). doi:10.1038/nbt.3805 Medline

13. S. Ausländer, D. Ausländer, M. Müller, M. Wieland, M. Fussenegger, Programmable single-cell mammalian biocomputers. *Nature* **487**, 123–127 (2012). doi:10.1038/nature11149 Medline

14. A. S. Khalil, T. K. Lu, C. J. Bashor, C. L. Ramirez, N. C. Pyenson, J. K. Joung, J. J. Collins, A synthetic biology framework for programming eukaryotic transcription functions. *Cell* **150**, 647–658 (2012). doi:10.1016/j.cell.2012.05.045 Medline

15. N. Roquet, A. P. Soleimany, A. C. Ferris, S. Aaronson, T. K. Lu, Synthetic recombinase-based state machines in living cells. *Science* **353**, aad8559 (2016). doi:10.1126/science.aad8559 Medline

16. L. B. Andrews, A. A. K. Nielsen, C. A. Voigt, Cellular checkpoint control using

programmable sequential logic. *Science* **361**, eaap8987 (2018). doi:10.1126/science.aap8987 Medline

17. B. Angelici, E. Mailand, B. Haefliger, Y. Benenson, Synthetic biology platform for sensing and integrating endogenous transcriptional inputs in mammalian cells. *Cell Rep.* **16**, 2525–2537 (2016). doi:10.1016/j.celrep.2016.07.061 Medline

18. J. J. Lohmueller, T. Z. Armel, P. A. Silver, A tunable zinc finger-based framework for Boolean logic computation in mammalian cells. *Nucleic Acids Res.* **40**, 5180–5187 (2012). doi:10.1093/nar/gks142 Medline

19. A. A. Green, P. A. Silver, J. J. Collins, P. Yin, Toehold switches: De-novo-designed regulators of gene expression. *Cell* **159**, 925–939 (2014). doi:10.1016/j.cell.2014.10.002 Medline

20. A. A. Green, J. Kim, D. Ma, P. A. Silver, J. J. Collins, P. Yin, Complex cellular logic computation using ribocomputing devices. *Nature* **548**, 117–121 (2017). doi:10.1038/nature23271 Medline

21. K. Rinaudo, L. Bleris, R. Maddamsetti, S. Subramanian, R. Weiss, Y. Benenson, A universal RNAi-based logic evaluator that operates in mammalian cells. *Nat. Biotechnol.* **25**, 795–801 (2007). doi:10.1038/nbt1307 Medline

22. L. Wroblewska, T. Kitada, K. Endo, V. Siciliano, B. Stillo, H. Saito, R. Weiss, Mammalian synthetic circuits with RNA binding proteins for RNA-only delivery. *Nat. Biotechnol.* **33**, 839–841 (2015). doi:10.1038/nbt.3301 Medline

23. S.-H. Park, A. Zarrinpar, W. A. Lim, Rewiring MAP kinase pathways using alternative scaffold assembly mechanisms. *Science* **299**, 1061–1064 (2003). doi:10.1126/science.1076979 Medline

24. P. L. Howard, M. C. Chia, S. Del Rizzo, F.-F. Liu, T. Pawson, Redirecting tyrosine kinase signaling to an apoptotic caspase pathway through chimeric adaptor proteins. *Proc. Natl. Acad. Sci. U.S.A.* **100**, 11267–11272 (2003). doi:10.1073/pnas.1934711100 Medline

25. B. Groves, A. Khakhar, C. M. Nadel, R. G. Gardner, G. Seelig, Rewiring MAP kinases in Saccharomyces cerevisiae to regulate novel targets through ubiquitination. *eLife* **5**, e15200 (2016). doi:10.7554/eLife.15200 Medline

26. L. Morsut, K. T. Roybal, X. Xiong, R. M. Gordley, S. M. Coyle, M. Thomson, W. A. Lim, Engineering customized cell sensing and response behaviors using synthetic Notch receptors. *Cell* **164**, 780–791 (2016). doi:10.1016/j.cell.2016.01.012 Medline

27. J. E. Dueber, B. J. Yeh, K. Chak, W. A. Lim, Reprogramming control of an allosteric signaling switch through modular recombination. *Science* **301**, 1904–1908 (2003). doi:10.1126/science.1085945 Medline

28. J. E. Dueber, E. A. Mirsky, W. A. Lim, Engineering synthetic signaling proteins with ultrasensitive input/output control. *Nat. Biotechnol.* **25**, 660–662 (2007). doi:10.1038/nbt1308 Medline

29. A. J. Smith, F. Thomas, D. Shoemark, D. N. Woolfson, N. J. Savery, Guiding biomolecular interactions in cells using de novo protein-protein interfaces. *ACS Synth. Biol.* **8**, 1284–1293 (2019). doi:10.1021/acssynbio.8b00501 Medline

30. X. J. Gao, L. S. Chong, M. S. Kim, M. B. Elowitz, Programmable protein circuits in living cells. *Science* **361**, 1252–1258 (2018). doi:10.1126/science.aat5062 Medline

31. T. Fink, J. Lonzarić, A. Praznik, T. Plaper, E. Merljak, K. Leben, N. Jerala, T. Lebar, Ž. Strmšek, F. Lapenta, M. Benčina, R. Jerala, Design of fast proteolysis-based signaling and logic circuits in mammalian cells. *Nat. Chem. Biol.* **15**, 115–122 (2019). doi:10.1038/s41589-018-0181-6 Medline

32. Z. Chen, S. E. Boyken, M. Jia, F. Busch, D. Flores-Solis, M. J. Bick, P. Lu, Z. L. VanAernum, A. Sahasrabuddhe, R. A. Langan, S. Bermeo, T. J. Brunette, V. K. Mulligan, L. P. Carter, F. DiMaio, N. G. Sgourakis, V. H. Wysocki, D. Baker, Programmable design of orthogonal protein heterodimers. *Nature* **565**, 106–111 (2019). doi:10.1038/s41586-018-0802-y Medline

33. K. E. Prehoda, J. A. Scott, R. D. Mullins, W. A. Lim, Integration of multiple signals through cooperative regulation of the N-WASP-Arp2/3 complex. *Science* **290**, 801–806 (2000). doi:10.1126/science.290.5492.801 Medline

34. B. Yu, I. R. S. Martins, P. Li, G. K. Amarasinghe, J. Umetani, M. E. Fernandez-Zapico, D. D. Billadeau, M. Machius, D. R. Tomchick, M. K. Rosen, Structural and energetic mechanisms of cooperative autoinhibition and activation of Vav1. *Cell* **140**, 246–256 (2010). doi:10.1016/j.cell.2009.12.033 Medline

35. K. N. Dyer, M. Hammel, R. P. Rambo, S. E. Tsutakawa, I. Rodic, S. Classen, J. A. Tainer, G. L. Hura, High-throughput SAXS for the characterization of biomolecules in solution: A practical approach. *Methods Mol. Biol.* **1091**, 245–258 (2014). doi:10.1007/978-1-62703-691-7_18 Medline

36. B. T. Ruotolo, C. V. Robinson, Aspects of native proteins are retained in vacuum. *Curr. Opin. Chem. Biol.* **10**, 402–408 (2006). doi:10.1016/j.cbpa.2006.08.020 Medline

37. Z. L. VanAernum, F. Busch, B. J. Jones, M. Jia, Z. Chen, S. E. Boyken, A. Sahasrabuddhe, D. Baker, V. H. Wysocki, Rapid online buffer exchange for screening of proteins, protein complexes and cell lysates by native mass spectrometry. *Nat. Protoc.* **15**, 1132–1157; Rapid online (2020). doi:10.1038/s41596-019-0281-0 Medline

38. A. Pause, B. Peterson, G. Schaffar, R. Stearman, R. D. Klausner, Studying interactions of four proteins in the yeast two-hybrid system: Structural resemblance of the pVHL/elongin BC/hCUL-2 complex with the ubiquitin ligase complex SKP1/cullin/F-box protein. *Proc. Natl. Acad. Sci. U.S.A.* **96**, 9533–9538 (1999). doi:10.1073/pnas.96.17.9533 Medline

39. B. Sandrock, J. M. Egly, A yeast four-hybrid system identifies Cdk-activating kinase as a regulator of the XPD helicase, a subunit of transcription factor IIH. *J. Biol. Chem.* **276**, 35328–35333 (2001). doi:10.1074/jbc.M105570200 Medline

40. A. S. Dixon, M. K. Schwinn, M. P. Hall, K. Zimmerman, P. Otto, T. H. Lubben, B. L. Butler, B. F. Binkowski, T. Machleidt, T. A. Kirkland, M. G. Wood, C. T. Eggers, L. P. Encell, K. V. Wood, NanoLuc complementation reporter optimized for accurate measurement of protein interactions in cells. *ACS Chem. Biol.* **11**, 400–408 (2016). doi:10.1021/acschembio.5b00753 Medline

41. Y.-C. Kwon, M. C. Jewett, High-throughput preparation methods of crude extract for robust

cell-free protein synthesis. *Sci. Rep.* **5**, 8663 (2015). doi:10.1038/srep08663 Medline

42. J. R. Porter, C. I. Stains, B. W. Jester, I. Ghosh, A general and rapid cell-free approach for the interrogation of protein-protein, protein-DNA, and protein-RNA interactions and their antagonists utilizing split-protein reporters. *J. Am. Chem. Soc.* **130**, 6488–6497 (2008). doi:10.1021/ja7114579 Medline

43. S. L. Maude, T. W. Laetsch, J. Buechner, S. Rives, M. Boyer, H. Bittencourt, P. Bader, M. R. Verneris, H. E. Stefanski, G. D. Myers, M. Qayed, B. De Moerloose, H. Hiramatsu, K. Schlis, K. L. Davis, P. L. Martin, E. R. Nemecek, G. A. Yanik, C. Peters, A. Baruchel, N. Boissel, F. Mechinaud, A. Balduzzi, J. Krueger, C. H. June, B. L. Levine, P. Wood, T. Taran, M. Leung, K. T. Mueller, Y. Zhang, K. Sen, D. Lebwohl, M. A. Pulsipher, S. A. Grupp, Tisagenlecleucel in Children and Young Adults with B-Cell Lymphoblastic Leukemia. *N. Engl. J. Med.* **378**, 439–448 (2018). doi:10.1056/NEJMoa1709866 Medline

44. S. S. Neelapu, F. L. Locke, N. L. Bartlett, L. J. Lekakis, D. B. Miklos, C. A. Jacobson, I. Braunschweig, O. O. Oluwole, T. Siddiqi, Y. Lin, J. M. Timmerman, P. J. Stiff, J. W. Friedberg, I. W. Flinn, A. Goy, B. T. Hill, M. R. Smith, A. Deol, U. Farooq, P. McSweeney, J. Munoz, I. Avivi, J. E. Castro, J. R. Westin, J. C. Chavez, A. Ghobadi, K. V. Komanduri, R. Levy, E. D. Jacobsen, T. E. Witzig, P. Reagan, A. Bot, J. Rossi, L. Navale, Y. Jiang, J. Aycock, M. Elias, D. Chang, J. Wiezorek, W. Y. Go, Axicabtagene Ciloleucel CAR T-Cell Therapy in Refractory Large B-Cell Lymphoma. *N. Engl. J. Med.* **377**, 2531–2544 (2017). doi:10.1056/NEJMoa1707447 Medline

45. J. A. Fraietta, S. F. Lacey, E. J. Orlando, I. Pruteanu-Malinici, M. Gohil, S. Lundh, A. C. Boesteanu, Y. Wang, R. S. O'Connor, W.-T. Hwang, E. Pequignot, D. E. Ambrose, C. Zhang, N. Wilcox, F. Bedoya, C. Dorfmeier, F. Chen, L. Tian, H. Parakandi, M. Gupta, R. M. Young, F. B. Johnson, I. Kulikovskaya, L. Liu, J. Xu, S. H. Kassim, M. M. Davis, B. L. Levine, N. V. Frey, D. L. Siegel, A. C. Huang, E. J. Wherry, H. Bitter, J. L. Brogdon, D. L. Porter, C. H. June, J. J. Melenhorst, Determinants of response and resistance to CD19 chimeric antigen receptor (CAR) T cell therapy of chronic lymphocytic leukemia. *Nat. Med.* **24**, 563–571 (2018). doi:10.1038/s41591-018-0010-1 Medline

46. C. H. June, R. S. O'Connor, O. U. Kawalekar, S. Ghassemi, M. C. Milone, CAR T cell immunotherapy for human cancer. *Science* **359**, 1361–1365 (2018). doi:10.1126/science.aar6711 Medline

47. A. H. Long, W. M. Haso, J. F. Shern, K. M. Wanhainen, M. Murgai, M. Ingaramo, J. P. Smith, A. J. Walker, M. E. Kohler, V. R. Venkateshwara, R. N. Kaplan, G. H. Patterson, T. J. Fry, R. J. Orentas, C. L. Mackall, 4-1BB costimulation ameliorates T cell exhaustion induced by tonic signaling of chimeric antigen receptors. *Nat. Med.* **21**, 581–590 (2015). doi:10.1038/nm.3838 Medline

48. E. J. Wherry, M. Kurachi, Molecular and cellular insights into T cell exhaustion. *Nat. Rev. Immunol.* **15**, 486–499 (2015). doi:10.1038/nri3862 Medline

49. E. J. Wherry, S. J. Ha, S. M. Kaech, W. N. Haining, S. Sarkar, V. Kalia, S. Subramaniam, J. N. Blattman, D. L. Barber, R. Ahmed, Molecular signature of CD8+ T cell exhaustion during chronic viral infection. *Immunity* **27**, 670–684 (2007). doi:10.1016/j.immuni.2007.09.006 Medline

50. K. E. Pauken, M. A. Sammons, P. M. Odorizzi, S. Manne, J. Godec, O. Khan, A. M. Drake, Z. Chen, D. R. Sen, M. Kurachi, R. A. Barnitz, C. Bartman, B. Bengsch, A. C. Huang, J. M. Schenkel, G. Vahedi, W. N. Haining, S. L. Berger, E. J. Wherry, Epigenetic stability of exhausted T cells limits durability of reinvigoration by PD-1 blockade. *Science* **354**, 1160–1165 (2016). doi:10.1126/science.aaf2807 Medline

51. M. S. Wilken, C. Ciarlo, J. Pearl, J. Bloom, E. Schanzer, H. Liao, S. E. Boyken, B. Van Biber, K. Queitsch, G. Heberlein, A. Federation, R. Acosta, S. Vong, E. Otterman, D. Dunn, H. Wang, P. Zrazhevskey, V. Nandakumar, D. Bates, R. Sandstrom, Z. Chen, F. D. Urnov, D. Baker, A. Funnell, S. Green, J. A. Stamatoyannopoulos, Regulatory DNA keyholes enable specific and persistent multi-gene expression programs in primary T cells without genome modification. bioRxiv 2020.02.19.956730 [Preprint]. 20 February 2020; https://doi.org/10.1101/2020.02.19.956730.

52. Z. Chen, R. D. Kibler, A. Hunt, F. Busch, J. Pearl, M. Jia, Z. L. VanAernum, B. I. M. Wicky, G. Dods, H. Liao, M. Wilken, C. Ciarlo, S. Green, H. El-Samad, J. Stamatoyannopoulos, V. H. Wysocki, M. C. Jewett, S. E. Boyken, D. Baker, Code used to simulate the cooperative binding system for: De novo design of protein logic gates, Zenodo (2020); https://doi.org/10.5281/zenodo.3697264.

53. S. E. Boyken, Z. Chen, B. Groves, R. A. Langan, G. Oberdorfer, A. Ford, J. M. Gilmore, C. Xu, F. DiMaio, J. H. Pereira, B. Sankaran, G. Seelig, P. H. Zwart, D. Baker, De novo design of protein homo-oligomers with modular hydrogen-bond network-mediated specificity. *Science* **352**, 680–687 (2016). doi:10.1126/science.aad8865 Medline

54. M. E. Lee, W. C. DeLoache, B. Cervantes, J. E. Dueber, A highly characterized yeast toolkit for modular, multipart assembly. *ACS Synth. Biol.* **4**, 975–986 (2015). doi:10.1021/sb500366v Medline

55. A. Aranda-Díaz, K. Mace, I. Zuleta, P. Harrigan, H. El-Samad, Robust synthetic circuits for two-dimensional control of gene expression in yeast. *ACS Synth. Biol.* **6**, 545–554 (2017). doi:10.1021/acssynbio.6b00251 Medline

56. F. W. Studier, Protein production by auto-induction in high density shaking cultures. *Protein Expr. Purif.* **41**, 207–234 (2005). doi:10.1016/j.pep.2005.01.016 Medline

57. J. K. Myers, C. N. Pace, J. M. Scholtz, Denaturant m values and heat capacity changes: Relation to changes in accessible surface areas of protein unfolding. *Protein Sci.* **4**, 2138–2148 (1995). doi:10.1002/pro.5560041020 Medline

58. P. Bernadó, M. Blackledge, J. Sancho, Sequence-specific solvent accessibilities of protein residues in unfolded protein ensembles. *Biophys. J.* **91**, 4536–4543 (2006). doi:10.1529/biophysj.106.087528 Medline

59. J. Estrada, P. Bernadó, M. Blackledge, J. Sancho, ProtSA: A web application for calculating sequence specific protein solvent accessibilities in the unfolded ensemble. *BMC Bioinform.* **10**, 104 (2009). doi:10.1186/1471-2105-10-104 Medline

60. R. P. Rambo, J. A. Tainer, Characterizing flexible and intrinsically unstructured biological macromolecules by SAS using the Porod-Debye law. *Biopolymers* **95**, 559–571 (2011). doi:10.1002/bip.21638 Medline

61. D. Schneidman-Duhovny, M. Hammel, A. Sali, FoXS: A web server for rapid computation

and fitting of SAXS profiles. *Nucleic Acids Res.* **38**, W540–W544 (2010). doi:10.1093/nar/gkq461 Medline

62. D. Schneidman-Duhovny, M. Hammel, J. A. Tainer, A. Sali, Accurate SAXS profile computation and its assessment by contrast variation experiments. *Biophys. J.* **105**, 962–974 (2013). doi:10.1016/j.bpj.2013.07.020 Medline

63. R. H. Schiestl, R. D. Gietz, High efficiency transformation of intact yeast cells using single stranded nucleic acids as a carrier. *Curr. Genet.* **16**, 339–346 (1989). doi:10.1007/BF00340712 Medline

64. C. T. Chien, P. L. Bartel, R. Sternglanz, S. Fields, The two-hybrid system: A method to identify and clone genes for proteins that interact with a protein of interest. *Proc. Natl. Acad. Sci. U.S.A.* **88**, 9578–9582 (1991). doi:10.1073/pnas.88.21.9578 Medline

65. P. L. Bartel, J. A. Roecklein, D. SenGupta, S. Fields, A protein linkage map of Escherichia coli bacteriophage T7. *Nat. Genet.* **12**, 72–77 (1996). doi:10.1038/ng0196-72 Medline

66. Z. L. VanAernum, J. D. Gilbert, M. E. Belov, A. A. Makarov, S. R. Horning, V. H. Wysocki, Surface-induced dissociation of noncovalent protein complexes in an extended mass range orbitrap mass spectrometer. *Anal. Chem.* **91**, 3611–3618 (2019). doi:10.1021/acs.analchem.8b05605 Medline

67. M. T. Marty, A. J. Baldwin, E. G. Marklund, G. K. A. Hochberg, J. L. P. Benesch, C. V. Robinson, Bayesian deconvolution of mass and ion mobility spectra: From binary interactions to polydisperse ensembles. *Anal. Chem.* **87**, 4370–4376 (2015). doi:10.1021/acs.analchem.5b00140 Medline

68. M. C. Jewett, J. R. Swartz, Mimicking the *Escherichia coli* cytoplasmic environment activates long-lived and efficient cell-free protein synthesis. *Biotechnol. Bioeng.* **86**, 19–26 (2004). doi:10.1002/bit.20026 Medline

69. A. D. Silverman, N. Kelley-Loughnane, J. B. Lucks, M. C. Jewett, Deconstructing cell-free extract preparation for in vitro activation of transcriptional genetic circuitry. *ACS Synth. Biol.* **8**, 403–414 (2019). doi:10.1021/acssynbio.8b00430 Medline

70. J. R. Swartz, M. C. Jewett, K. A. Woodrow, in *Recombinant Gene Expression: Reviews and Protocols*, P. Balbás, A. Lorence, Eds. (Human, 2004), pp. 169–182.

71. V. Muñoz, L. Serrano, Elucidating the folding problem of helical peptides using empirical parameters. III. Temperature and pH dependence. *J. Mol. Biol.* **245**, 297–308 (1995). doi:10.1006/jmbi.1994.0024 Medline